https://doi.org/10.5194/egusphere-2024-4023
Preprint. Discussion started: 19 March 2025

Connecting Deep Aquifer Recharge in California's Central Valley to Sierra Nevada Snowmelt via Multi-Sensor Remote Sensing Data

Susanna Werth[1], Manoochehr Shirzaei[1,2,3], Grace Carlson[1,4], and Roland Bürgmann[5]

[1]Virginia Tech, Department of Geosciences, Blacksburg, VA, USA.
[2]Virginia Tech, National Security Institute, Blacksburg, VA, USA.
[3]United Nations University, Institute for Water, Environment and Health, Hamilton, ON L8P 0A1, Canada
[4]University of California, Berkeley, Department of Environmental Science, Policy, and Management, Berkeley , CA, USA
[5]University of California, Berkeley, Department of Earth and Planetary Science, Berkeley, CA, USA.

Correspondence to: Susanna Werth (swerth@vt.edu)

Abstract. California's arid Central Valley (CV) relies on groundwater pumped from deep aquifers (i.e., >50m) and surface water transported from the Sierra Nevada to produce a quarter of the United States' food demand. Similar to other basin aquifers adjacent to high mountains, the natural recharge to CV's deep aquifers is thought to be regulated by the adjacent high mountains of the Sierra Nevada, but the underlying mechanisms remain elusive. We investigate large sets of geodetic remote sensing, hydrologic, and climate data and employ a first-order model assessment at annual time scales to investigate possible recharge mechanisms. Peak annual groundwater storage in the CV lags several months behind groundwater levels, suggesting a longer transmission time for water flow than pressure propagation. We further find that peak groundwater levels lag the Sierra Nevada snowmelt by about one month, consistent with an ideal fluid pressure diffusion time in the Sierra's fractured crystalline body. Our results suggest that high mountain snowpack changes likely impact freshwater availability in the basin aquifers. Our analysis and a first-order pressure propagation model link the current precipitation and meltwater in the high mountain Sierra to deep CV aquifers through mountain block recharge process, highlighting the importance of longer groundwater flow paths through bedrocks for recharging deep aquifers in CV and other basin aquifer systems adjacent to mountains globally. This underscores the need for new hydroclimate models to fully account for the role of high mountains in lowland water cycles by including mountain block recharge, and revision of current management and drought resiliency plans in California.

1 Introduction

The global availability of groundwater is threatened by excess pumping and climate change. During a dry year, up to 70% of the groundwater used in the Central Valley (CV), California, is pumped within the growing season, mainly between April and June (Faunt, 2009), causing a long-term decline in groundwater levels, with the fastest rates observed in the southern San Joaquin basin, including the Tulare basin (Fig. 1a) (Faunt, 2009; Faunt et al., 2016; Konikow, 2015; Massoud et al., 2018; Ojha et al., 2018). Given the poor quality of shallow water in the southern CV (Hanak et al., 2017), most groundwater

https://doi.org/10.5194/egusphere-2024-4023
Preprint. Discussion started: 19 March 2025

demand is addressed by tapping into deep aquifers at ~50 m to ~500 m depth below the surface (see Fig. 1b in Perrone & Jasechko, 2019), which are overlain by the confining layer of the Corcoran Clay and widespread clay lenses (Faunt, 2009) (Fig. 1a). While not continuous, taken all of the lenses together, they significantly reduce the vertical hydraulic conductivity (Faunt, 2009). Recharge via direct percolation of surface water vertically into several hundred meters deep (semi-)confined aquifers of the CV through impermeable Corcoran Clay layer or clay lenses is implausible, at least at the time scale of a month to a year (Shirzaei et al., 2019), corroborated by groundwater-age data (McMahon et al., 2011). For instance, Burow et al., (2007) reported a recharge rate of less than 600 mm/yr for unconfined aquifers in San Joaquin Valley, which allows a link between the water table in unconfined aquifers and the surface water on an annual time scale (Brush et al., 2013).

Understanding key natural and artificial processes in recharging aquifer systems is essential for sustainable water management to store water for future use (Escriva-Bou et al., 2020, 2021; Ghasemizade et al., 2019). Planned or intentional replenishment of aquifers by using surplus water (e.g., floodwater) through so-called managed aquifer recharge (MAR) is a successful adaptation strategy that banks water to be used later, for instance, during droughts (Dillon, 2005; Jakeman et al., 2016; Zheng et al., 2021), which mitigates negative impacts of climate change on the groundwater resources. In arid and semiarid regions, such as the lowland Central Valley (CV) adjacent to the Sierra Nevada (Fig. 1a), the availability of surplus water, in addition to other factors, such as geomorphology, hydrology, soil conditions, land use, and economic conditions, determine the success of MAR and the effective recovery of head levels (Ghasemizade et al., 2019; Kourakos et al., 2019, 2023; Marwaha et al., 2021). For instance, Kourakos et al. (2019) show that using the CV's irrigated agricultural areas as potential sites for MAR allows efficient storage of large volumes of water only during long recharge periods due to low diversion rates. The contribution of intentional recharge to CV's aquifers through basins, unlined canals, and injection is likely small due to the natural disconnect between groundwater overdraft in dry areas and surface water surplus in wet areas (Alley, 2002; Ayres et al., 2021; Escriva-Bou et al., 2021; Siebert et al., 2010; Zektser & Everett, 2004). Thus, large-scale natural recharge to deep (semi-) confined aquifers below 50 m depth is essential for replenishing dryland groundwater resources. In contrast to artificial recharge, the mechanisms of natural recharge to deep aquifers remain elusive in the CV.

California's wet and dry seasons occur during November-April and May-October, respectively, with a large portion of the Sierra Nevada's precipitation falling as snow during the winter that supplies snow melt in spring (Fig. S1, S2). The Sierra Nevada's snowpack is thought to regulate surface water availability in the CV during the summer (Faunt, 2009; Peterson et al., 2003; Urióstegui et al., 2017). Isotope studies and streamflow analysis of snow-dominated mountainous watersheds of the western USA suggest that snowpacks via snowmelt significantly contribute to groundwater recharge, depending on existing geology (Earman et al., 2006; Tague et al., 2008; Tague & Grant, 2009). However, the mechanisms linking the Central Valley's deep aquifer recharge to precipitation, underground storage, and water transport in the Sierra Nevada are not well-established and disputed in the literature (Huth et al., 2004; Jódar et al., 2017; Liu et al., 2017).

https://doi.org/10.5194/egusphere-2024-4023
Preprint. Discussion started: 19 March 2025

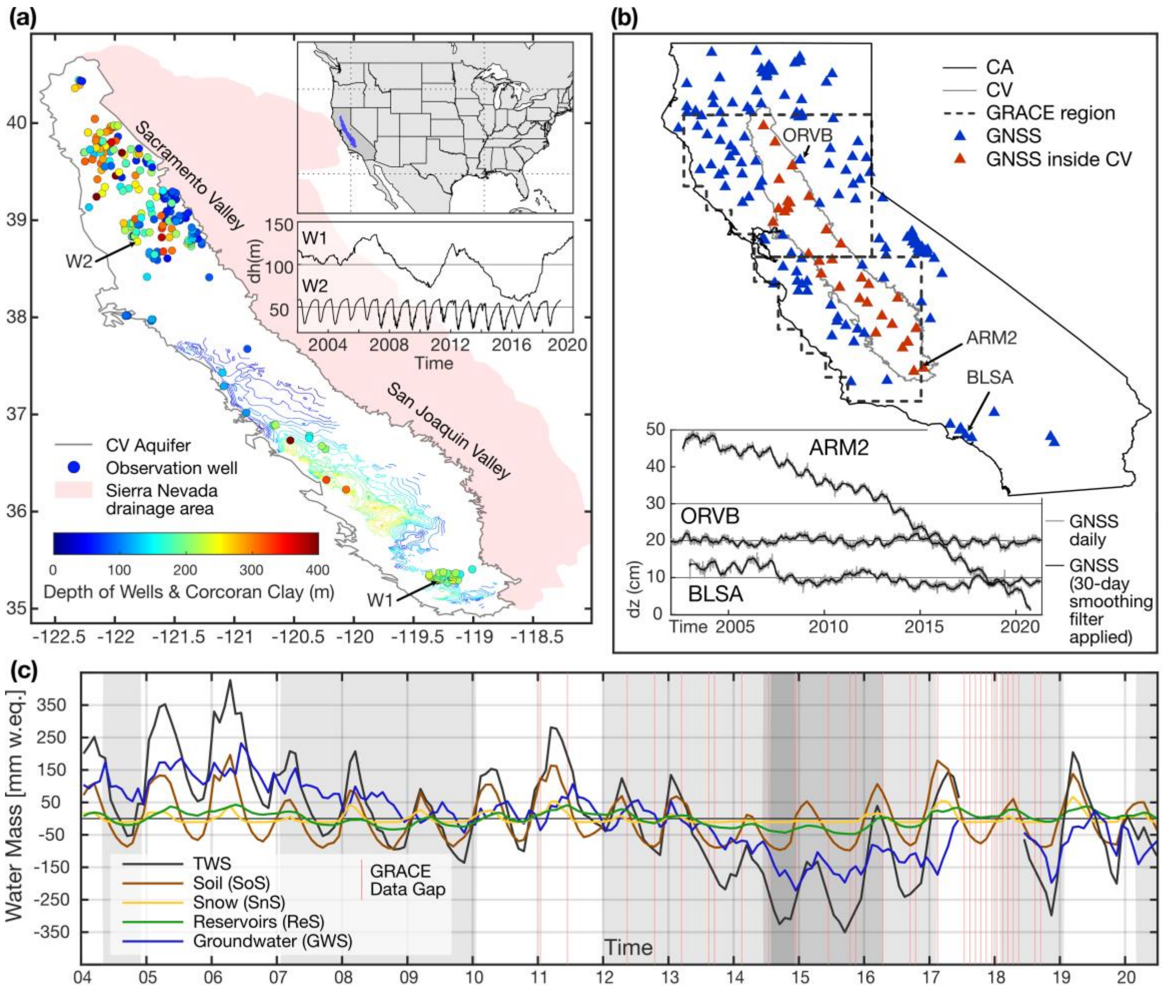

Figure 1: Overview of study area and data sets applied in this study. (a) Study area and hydrogeological datasets: Outline of the Central Valley aquifer system (grey line, $A_{CV} = 53{,}672$ km2), Sierra Nevada drainage area (red shade, $A_{SN} = 63{,}780$ km2), location and depth of observation wells that provide measurements at depth of 50 m and deeper, and lateral coverage and depth of the confining Corcoran clay layer (source USGS: https://water.usgs.gov/GIS/metadata/usgswrd/XML/pp1766_corcoran_clay_depth_feet.xml). See Figure S4e and S4f for histograms of well depths. Top inset indicates location of the study area over contiguous US. Bottom inset shows time series of two selected well sites W1 (#352958N1193011W001) and W2 (#387793N1218123W004). (b) Geodetic data sets: Mass change regions of JPL GRACE mascon solutions (black dashed line) and location of GNSS sites from the University of Reno, Nevada (red and blue triangles). Red triangles mark stations located inside the Central Valley (CV), and blue triangles those outside the CV aquifer boundary. (c) Time series of TWS from GRACE, composite hydrological storages and estimated GW storages are averaged for the GRACE region shown in panel a, after Ojha et al. [2019]. Gray shaded background areas (light, medium, dark gray) indicate that the USDM identifies >30% (>30%, >60%) of California's area to be in moderate (exceptional, exceptional) dry condition (compare Fig. S3).

Given the low flow velocity of water underground, deep valley aquifers adjacent to high mountains, such as the CV, are thought to be recharged by lateral flows from higher elevations (Feth, 1964). The two main processes considered are Mountain Front Recharge (MFR) and Mountain Block Recharge (MBR, Fig. 2) (Somers & McKenzie, 2020). MFR often

https://doi.org/10.5194/egusphere-2024-4023
Preprint. Discussion started: 19 March 2025

directly recharges shallow, unconfined aquifers and causes a rise in the water table near streambeds from the mountain front to the basin aquifer (e.g. Visser et al., 2018). MBR replenishes deeper, often confined, and semi-confined aquifers laterally connected to high mountain aquifers (Somers & McKenzie, 2020). MBR occurs through fractures in the mountain block hydraulically connected to deep valley aquifers. Despite their proximity, there is no consensus on the role of MBR from the Sierra Nevada's granitic bedrock block into the CV aquifers; thus, it is not considered explicitly in current large-scale hydrological models used in water management assessments (Faunt, 2009; Hanson et al., 2012; Markovich et al., 2019). Meixner et al. (2016) lumped both processes into mountain system recharge (MSR) and estimated that it accounts for ~20% of total GW recharge in the CV, the rest being diffuse and irrigation recharge processes in shallow layers. Recent modeling experiments indicate that MFR drives almost all of the MSR to the CV aquifers (Schreiner-McGraw & Ajami, 2022). However, another study based on hydrological modeling concludes that MBR is more important and contributes up to 23% of the total GW recharge to the CV (Gilbert & Maxwell, 2017). A more recent study suggests a greater hydraulic conductivity between the Sierra Nevada and the Central Valley aquifers, and the authors determine, based on hydrochemical and isotope data, that up to 50% of the CV groundwater recharge sources from MBR (Armengol et al., 2024). These hydrogeological studies generally agree on the role of MSR components. However, they disagree on the importance of MBR for recharging deep valley aquifers of the CV, while the spatial extent of their investigations remains at scales of smaller watersheds that do not cover the entire CV.

An observation of groundwater volume change at the scale of the CV is available from remote sensing techniques, e.g., via their impact on the gravity field observed by the Gravity Recovery And Climate Experiment (GRACE) and on surface deformation observations with Global Navigation Satellite System (GNSS) or Interferometric Synthetic Aperture Radar (InSAR). Some studies, e.g., Neely et al. (2021) analyzing high-resolution deformation maps, suggest direct recharge of deep aquifers at the mountain front following heavy precipitation events and surface water supply surplus during wet years. These studies focus on local features below alluvial fan units along the mountain front, and not on areas with impermeable clay layers separating shallow and deep aquifers (Faunt, 2009; Shirzaei et al., 2019). There is no evidence of vertical fractures (Carlson, Shirzaei, Ojha, et al., 2020) in the CV to provide a direct pathway for the downward flow of surface water. Argus et al. (2022) use remote sensing data and hydrological models to quantify MBR from the Sierra Nevada to the CV at about 5 km^3/yr, though they do not discuss possible contributions from MFR and do not provide a conceptual or physical model describing the deep aquifer recharge mechanisms.

Understanding the spatiotemporal relationship between California's high mountains and deep valley aquifers is essential for developing appropriate plans supporting sustainable groundwater use. In the climate change era, when drought frequency and intensity have increased globally (Fox-Kemper et al., 2021), including in California (Fig. S3), elevation-dependent warming (Pepin et al., 2015) disproportionally impacts the water availability and storage in high mountains. During the last decades, increased evapotranspiration, decreased or delayed precipitation, and snowfall have caused severe snow droughts in the western USA, including the Sierra Nevada (Harpold et al., 2017; Hatchett & McEvoy, 2018; Mote et al., 2018). The low-snow years are expected to occur more regularly in the coming decades (Siirila-Woodburn et al., 2021). These droughts also

https://doi.org/10.5194/egusphere-2024-4023
Preprint. Discussion started: 19 March 2025

reduce the supply for mountain system recharge. Ignoring the MBR contribution, if relevant, may cause an overestimation of the lowland aquifer resilience to climate change and excess freshwater demand.

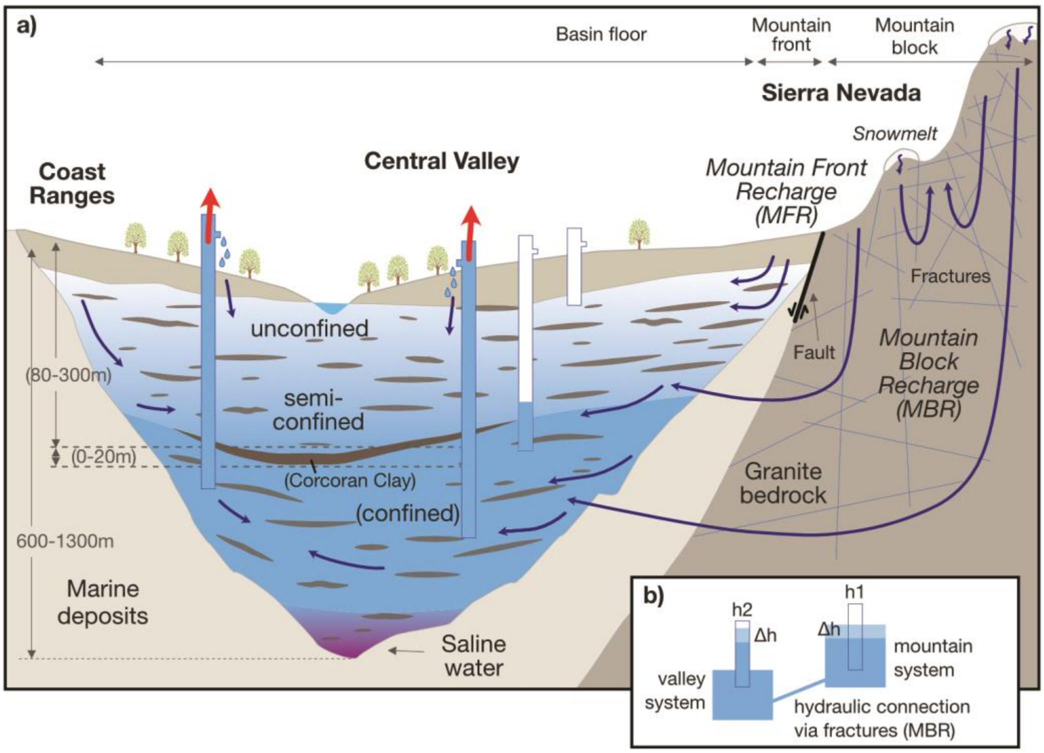

Figure 2. Conceptual and process-based sketch of pressure propagation and recharge in the Sierra Nevada to deep aquifer layers of the Central Valley. (a) Hydrogeological setting in the Central Valley (~400 m a.s.l.) and Sierra Nevada (up to ~4000 m a.s.l.). Indicated are major groundwater fluxes in and out from deep aquifer layers, including mountain front and mountain block recharge (MFR and MBR). Confining unit of the Corcoran clay is only present in the southern San Joaquin Valley, where pumping is more intense compared to the northern Sacramento Valley (Fig. 1a). This graph is inspired by Faunt et al. (2009) (Fig. A9 therein), Smith et al. (2017) (Fig. 2 therein) as well as Somers and McKenzie (2020) (Fig. 5 therein). b) Simplified conceptual sketch focusing on the MBR system. The two aquifer systems, the valley and mountain aquifers, are hydraulically connected via fractures in the mountain block. The mountain system is elevated with respect to the valley system generating recharge from the mountains toward the valley system. A change in the pressure head (h1) in the mountain system would lead to a change in the pressure head of the valley system (h2). The pressure change in the mountain propagates according to Equation (1) and in 1D simplification according to Equation (4) to depth, independent from the cross-sectional area of the conduit, and it precedes the actual flow of water volume (mass) that is dependent on the cross-sectional area of the conduit.

Here, we aim to identify evidence of MBR through a corroborative analysis of available observations, which measure various physical signatures of groundwater dynamics. Our approach complements the existing body of research on MBR in the Central Valley by drawing a big picture of the annual groundwater dynamics across the entire Central Valley. To that end, we apply a robust data-driven statistical framework and wavelet-based signal decomposition schemes to investigate seasonal variations in several geodetic remote sensing and hydrologic datasets across the CV and the Sierra Nevada,

https://doi.org/10.5194/egusphere-2024-4023
Preprint. Discussion started: 19 March 2025

potentially linked to the dynamics of groundwater volume change at a large scale. The data sets include groundwater level (GWL, Fig. 1a, S4), surface deformation from Interferometric Synthetic Aperture Radar (InSAR) and Global Navigation Satellite System (GNSS) (Fig. 1b, S5), Gravity Recovery and Climate Experiment (GRACE) satellite-derived total water storage (TWS) variations, soil water storage (SoS), snow storage (SnS) and reservoir storage (ReS, Fig. 1c). Next, through sophisticated time-frequency and correlation analysis, we identify hidden and non-stationary patterns in time series, quantifying their relationships. We further present a first-order diffusion model to examine the feasibility of the relationships inferred by our data-driven analysis. Our analysis and results highlight the importance of MBR in addition to MFR for CV deep aquifer recharge.

2 Data and Methods

2.1. Water Storage Components, Precipitation, and Snow Melt

GRACE and GRACE Follow-on missions (hereafter referred to as simply GRACE) monitor monthly changes in the Earth's gravity field at a spatial resolution of ~300-400 km, which are converted to equivalent total water storage (TWS) changes close to the surface (Schmidt et al., 2008; Tapley et al., 2004). In California, associated mass variations can be attributed to the terrestrial water cycle dynamics at sub-seasonal to interdecadal time scales. Water flow processes on and below the surface change the region's total amount of water stored in the soil, snowcap, surface- (including reservoirs and rivers), and groundwater. With that, GRACE total water storage variations reflect water loss, e.g., due to drought or human activities like intense groundwater pumping, as a mass deficit. Vice versa, for wetter periods, the surplus of water is detected. This allows for predicting groundwater storage in large aquifers if storage changes in all other components can be quantified and removed from GRACE TWS (Famiglietti et al., 2011; Scanlon et al., 2012).

Here, we derive groundwater storage (GWS) changes from GRACE observations using an approach similar to Ojha et al. (2019). We retrieve GRACE TWS variations from the RL06 Level-3 product from NASA's Jet Propulsion Laboratory (JPL) that solves regional mass variations at a resolution of 3-degree. JPL applies a coastal resolution filter for mascon cells at the coast that corrects for signal leakage into oceans, which is why the mascon cells we use here for the CV are cut off at the coast, as shown in Figure 1b. We do not apply JPL-mascon scale factors, as we calculate groundwater changes at this native resolution, and we assume leakage between the mascon tiles to be neglectable. A linear interpolation is applied to oversample GRACE data from their original irregular monthly sampling to a regular monthly time series before further combining them with other datasets. To separate GWS changes from GRACE TWS, we retrieve mass variations in other storage compartments from multiple data sets. We acquire soil moisture variations from all available soil layers in the NOAH, CLSM and VIC models of the Global Land Data Assimilation System (GLDAS) Version 2.1 (Beaudoing et al., 2016; Rodell et al., 2004) at 0.25 (Noah) and 1-degree (CLSM and VIC) resolution, respectively, for the entire GRACE period. We average the three models to one ensemble dataset for further analyses after resampling them to a uniform 0.5-degree resolution (Fig. 1c). For comparison, we also retrieve soil storage changes from the WaterGAP Global Hydrological

https://doi.org/10.5194/egusphere-2024-4023
Preprint. Discussion started: 19 March 2025

Model (WGHM, version 2.2d) at 0.5-degree resolution, which is available until 2016 (Fig. S12a). We integrate reservoir storage (ReS) changes from 18 reservoirs with capacities larger than or equal to 0.9 km^3, inside the margins of the two mascon cells covering the CV (GRACE region, Fig. 1b), which are retrieved from the California Department of Water Resources (CDWR, 2017). Snow storage (SoS) changes are acquired in the form of snow water equivalent from the Snow Data Assimilation System (SNODAS) (NOHRSC, 2004) over the contiguous United States since the end of 2003. A recent comparison of operational and retrospective model datasets for the western United States indicates differences in the spatial distribution of the snow cover toward airborne snow observatory data (Yang et al., 2023). However, these do not significantly impact the timing of maximum SoS based on spatial averages for the Sierra Nevada Region, as we apply them here (see Fig. 7 therein). Monthly water mass variations for each storage compartment are summed across the GRACE region, and the regionally aggregated SoS, SnS and ReS variations are removed from GRACE TWS variations after Ojha et al. (2019). The resulting time series for each storage compartment, including groundwater storage changes during both GRACE mission periods, are shown in Figure 1c. We assume the GRACE-based GWS estimate is dominated by groundwater variations in the CV, where aquifer storage capacity is likely much larger than that in the SN Mountains.

From the SNODAS dataset, we further retrieve driving and output variables related to snow cover, including ‘solid’- and ‘liquid precipitation’, and ‘snowmelt runoff at the base of the snowpack’, to investigate these fluxes in the Sierra Nevada (Fig. S1, S2) and their correlation to groundwater dynamics.

2.2. Groundwater Levels

Groundwater availability in the CV is conventionally monitored as water level changes in observation and irrigation wells. The data archives from the United States Geological Survey (USGS) and the California Department for Water Resources (CDWR) provide more than 40,000 records from wells within the CV. The records have varying start dates, not all are continuously monitored until today, and only some records provide sufficient temporal sampling rates to study seasonal variations in GWLs. For this study, we have screened ‘daily data’ and ‘field data’ archives from the USGS (USGS, 2021) as well as ‘continuous data’ and ‘periodic data’ archives from CDWR (CDWR, 2019a) in California and selected records that cover the GRACE mission period from 2002 to 2020. We have excluded records labeled as ‘irrigation well’ and only selected sites labeled ‘observation well’. This significantly reduces the amount of data points, especially in the south. However, water levels in observation wells are less likely affected by the localized reduction in pressure during and after pumping from the well, which is an important criterion. Levels in observation wells are more likely to represent a regional state of pressure and storage changes in the entire aquifer. In addition, we categorized data entries that are larger than 3.5 times the standard deviation of the detrended time series as outliers and excluded them. Moreover, about half of the records have daily sampling rates, and we excluded entire records from the field/periodic datasets, which had less than six entries per year on average. From the initial dataset, 2128 time series (371 from USGS and 1727 from CDWR) provide observation records from 2002-2020 inside the CV. Only 682 records cover at least three years with less than 3 months of gap (Fig. S4).

https://doi.org/10.5194/egusphere-2024-4023
Preprint. Discussion started: 19 March 2025

We remove well measurements taken at depths shallower than 50 m to exclude the bulk of wells that likely tap into unconfined layers and are located above clay lenses distributed throughout the Central Valley aquifer, creating (semi-) confined conditions. We are left with 457 records gathered at depths deeper than 50 m, allowing us to focus on measurements made in semi-confined and confined aquifers. About half of these records are longer than 10 years (Fig. S4a-c), and their average depth is 155 m. We note that these records were taken at only 250 unique well locations (circles in Fig. 1a), with some sites containing up to five nested level meters (Fig. S4d). Most of the lowest sensors at each site are located 50 m to 300 m below the surface, with about half of the sensors reaching not more than 200 m deep and only a few are 450 m deep or deeper (Fig. 1a, S4e, f). The average depth of the lowest sensor at unique well locations is 180 m. Most usable wells are in the northern Sacramento Valley, and only two dozen sites are in the southern San Joaquin Valley, where only 22 wells measure water level variations at depths below the Corcoran clay, and most of them fall into the eastern slope of the basin, between the Sierra Nevada and the deepest point of the Corcoran Clay and Valley. Examples of GWL time series are shown in Figure 1a.

2.3. Surface Deformation

Surface deformation due to TWS change, including GWS, occurs through two different processes. Total water mass deforms Earth's elastic crust, resulting in subsidence for an increase and uplift for a decrease in water mass. This deformation process has been described and inverted to quantify TWS in California (Adusumilli et al., 2019; Argus et al., 2022; Borsa et al., 2014; Carlson et al., 2022; Carlson, Shirzaei, Werth, et al., 2020; White et al., 2022). A second poroelastic deformation process is due to only groundwater changes occurring in semi-confined or confined aquifers, where pore spaces and granular matrix of rocks compact and groundwater levels fall under reduced water pressure. The opposite happens for increasing water pressure. The poroelastic deformation of unconfined aquifers is negligible due to relatively small values of the Biot-Willis coefficient linking fluid pressure to solid matrix confining stress (Wang, 2000), which we demonstrated in Supplementary Text S1. Changes in water pressure in a confined aquifer can either be caused by net recharge or discharge, i.e. GWS change, in the aquifer itself, or initiated by water pressure propagating between the aquifer and a hydraulically connected outside region (Fetter & Kreamer, 2022). Decades of falling groundwater levels in the CV deep aquifers have caused continuous land subsidence at the surface and have been observed to be most severe during droughts (Galloway et al., 1999; Ojha et al., 2018; Smith et al., 2017; Vasco et al., 2022). It has been shown that elastic loading deformation in California is of the opposite sign and up to two magnitudes smaller than the poroelastic deformation occurring at the surface of the CV (Carlson, Shirzaei, Werth, et al., 2020).

To study seasonal variations in vertical land motion (VLM) since the early 2000s, we use vertical deformation time series from the daily tenv3 GNSS solutions from the Nevada Geodetic Laboratory (NGL). The solutions are processed at NGL using GipsyX software and are transformed into the IGS14 reference frame. Additional processing information can be found on the NGL website (http://geodesy.unr.edu/gps/ngl.acn.txt). We do not apply any further corrections to the GNSS time

https://doi.org/10.5194/egusphere-2024-4023
Preprint. Discussion started: 19 March 2025

series for the rest of our analysis. From 1184 stations in California, we selected 170 with a minimum record of 5 years between 2002-2020 and exhibiting a seasonal amplitude larger than the time series median standard deviation. This selection criterion discards stations with near zero seasonal amplitude and those with observations dominated by noise, mainly located outside confined aquifer areas. Most selected stations began observations around 2008, lasting 15 years (Fig. S5b). Of these stations, 37 are located within the CV boundaries (red triangles, Fig. 1b). Example time series at three sites throughout the study area are shown in the inset of Figure 1b. Using a time-frequency analysis, we determine the seasonal component of GNSS vertical land motion and the timing of maximum uplift and subsidence (see Section 2.4).

We further measure the surface deformation in terms of line-of-sight (LOS) over the southern CV using Interferometric Synthetic Aperture Radar (InSAR). The SAR dataset includes 238 C-band images from descending track, path 144, of Sentinel-1A/B satellites spanning 2015/11/27-2022/12/20. We apply multi-looking factors of 32 and 6 in range and azimuth to obtain a pixel dimension of ~75m by ~75m. We use GAMMA software (Werner et al., 2000) to create a large set of interferograms. The interferograms are selected so they form triplets, and the numbers of short, medium, and long temporal baseline pairs are comparable to minimize the phase closure error impact (Lee & Shirzaei, 2023). We apply the wavelet-based InSAR (WabInSAR) (Lee & Shirzaei, 2023; Shirzaei, 2013; Shirzaei et al., 2017) algorithm to perform a multitemporal interferometric analysis of the SAR dataset and create high-accuracy maps of surface deformation time series. A Shuttle Radar Topography Mission (SRTM) Digital Elevation Model (DEM) of 1-arcsecond (~30 m) spatial resolution (Farr et al., 2007) and precise satellite orbital information are used to estimate and remove the effect of topographic phase and flat earth correction (Franceschetti & Lanari, 1999). The absolute phase values are obtained by applying a 2D minimum cost flow algorithm (Costantini, 1998), then combined to create a Line-of-Sight (LOS) time series of surface deformation using a reweighted least squares approach. The spatially correlated and temporally uncorrelated atmospheric delay are also estimated and removed (Shirzaei, 2013).

2.4. Time-Frequency Analysis

To investigate the temporal variations in water storage components, GWLs, and deformation data, we perform a time-frequency analysis using a continuous wavelet transform, following Shirzaei et al. (2013). The wavelet transform allows decomposing signals into building blocks based on frequency contents. In contrast to the Fourier transforms, the wavelets can handle non-stationary signals and localize the signal energy in the time and frequency domain (Goswami & Chan, 1999). Wavelets have a key parameter scale (or dilation), which stretches or squishes the wavelet function and relates to the analyzed signal frequency. To perform wavelet analysis, we use the Matlab packages provided by Torrence and Compo (1998) and Erickson (2019) and apply the wavelet family of derivatives of Gaussian (DOG, Fig. S6) at 200 levels of decomposition or scales. The temporal sampling of all time series is either daily or resampled at daily intervals using linear interpolation.

https://doi.org/10.5194/egusphere-2024-4023
Preprint. Discussion started: 19 March 2025

Figures 3 and S7 illustrate our approach with an example of groundwater level time series at the DWR well #387793N1218123W004 (Fig. S7a). The wavelet power spectrum map (PSM, Fig. 3a and S7b) shows the signal's energy breakdown into several frequency components and their relative importance based on the amplitude of the PSM. A cone-of-influence overprinted on the spectrum indicates areas where edge effects play a role, and therefore, the PSM cannot be interpreted. Signal energy in areas inside the cone of influence is strongest at periods of about one year, with contour lines indicating their statistical significance with respect to white and red noise (with a lag-1 autocorrelation parameter of 0.85 for the latter) (Torrence & Compo, 1998). Figure 3 also shows examples of wavelet PSM for selected GWL, VLM, and TWS component time series.

To isolate the annual component from the time series, we set the PSM to zero except for periods between 0.75-1.25 years and then apply an inverse wavelet transform of the new PSM (Fig. S7c). This approach considers that the annual components in climate-related processes do not have an exact one-year period. We further analyze the reconstructed annual signals to characterize the timing of annual maxima, minima, and the timing of fastest rate declines and increases (blue, red, and gray circles in Fig. S7c). We summarize the annual values for several years through temporal averaging using the median operator to retrieve the timing of maximum in the annual signal (e.g., as shown in Fig. 4). We successfully apply this method to time series of original daily to monthly temporal sampling resolution, after oversampling all datasets for a regular daily time series using linear interpolation (see example for original monthly time series from well #387626N1213651W002 in Fig. S7d-f). The same approach is applied to the time series of GWL, TWS components, GNSS and InSAR vertical deformation.

Probability density functions (PDFs) for spatiotemporal variation of timing of annual peaks were calculated using MATLAB's probability density estimator *kdensity()*, based on a normal kernel function for univariate distributions and applies a kernel smoothing window with an optimized bandwidth for normal densities. Since sample sizes are much larger than the minimum of ~30 suggested by the central limit theorem (Meyer, 1970), the outcome of the statistical analysis is independent of the assumed distribution (e.g., normal) of the individual samples. Thus, choosing a normal kernel function has no impact on the results.

2.5. Vertical Diffusion Model to Propagate Pressure from Mountains to Valley

In the high Sierra Nevada, a significant portion of snow melt water (Fig. S1, S2) infiltrates into the ground and recharges top aquifer layers (Peterson et al., 2003; Urióstegui et al., 2017), which are hydraulically connected to the CV aquifer system (Faunt, 2009), via fractures in the mountain front and the mountain block (Fig. 2a). In this study, we focus on mountain block recharge that acts at deeper depth and thus longer paths. The mountain block fractures provide hydraulic connectivity between elevated mountain aquifers and the valley system, as further highlighted by a simplified sketch in Figure 2b. Hence, a change in the pressure head (h_{p1}) in the mountain system would lead to a change in the pressure head of the valley system (h_{p2}). A pressure increase precedes the groundwater flow, which can initiate fluid diffusion from one location to another.

https://doi.org/10.5194/egusphere-2024-4023
Preprint. Discussion started: 19 March 2025

While related, pressure (or pressure propagation) and storage (or mass) change are physical phenomena that follow distinct mathematical equations and occur over different time scales. The temporal evolution of pressure ($\frac{dP}{dt}$) follows:

$$\frac{dP}{dt} = \kappa \cdot \nabla^2 P \; , \tag{1}$$

where the hydraulic diffusivity $\kappa = K/S_s$, controling the speed of pressure propagation, is the ratio of vertical hydraulic conductivity K to specific storage S_s. On the other hand, the law governing groundwater flow (i.e., mass transport) is provided by Darcy's equation:

$$q = -K \cdot \nabla P, \tag{2}$$

where q is flux per unit area and assuming groundwater volume flow $Q = q \cdot A$ and with $K = \kappa \cdot S_S$ Equation (2) can be rewritten as:

$$Q = \frac{dV}{dt} = -\kappa \, S_S \, A \cdot \nabla P \; . \tag{3}$$

Equation (3) illustrates that the groundwater flow depends on the cross-sectional area of the flow path and the specific storage coefficient, both of which are small for the mountain block. For fractured bedrock S_S has magnitudes as small as 10^{-5} to 10^{-6}. In contrast, pressure propagation is independent of these two factors. Hence, the recovery of the water storage in the valley due to the water transport from the mountain through fractures must take much longer than the pressure front propagation (Viswanathan et al., 2022). At the annual time scale, this can cause a change in the pressure head without causing a significant change in the valley storage. However, in this study, we are mainly interested in the annual propagation of a pressure front resulting from snow melt and winter rain. Hence, we only investigate the time it takes for a pressure front to propagate vertically from the mountains to deep layers, i.e., depths below the Corcoran clay, of the valley aquifer system.

Here, to obtain the first-order approximation of the diffusion time, namely the time it takes for snow melt-related pore-fluid pressure increase in the Sierra to reach deep aquifer layers of the CV via MBR, we apply the 1D form of the Equation (1) following (Saar & Manga, 2003). Hence, the vertical propagation of hydrostatic pore-fluid pressure P at depth z over time t is governed by the diffusion equation:

$$\kappa \frac{\partial^2 P}{\partial z^2} = \frac{dP}{dt} \, . \tag{4}$$

and the hydraulic diffusivity κ controls how fast pressure will propagate to depth. The diffusivity of unfractured granite bedrock has values of around $\kappa = 10^{-4}\ m^2/s$ (Wang, 2000). However, for fractured volcanic rock, values as high as 0.3 m^2/s (Saar & Manga, 2003), and 1 m^2/s (Gao et al., 2000), consistent with the range provided by Talwani and Acree (1985), or even up to 7.9 m^2/s (Montgomery-Brown et al., 2019) are suggested. The true diffusivity values are highly uncertain, as MBR likely occurs through conduits with secondary porosity, and their contribution may be underestimated at a large scale and, therefore, not be reflected accurately in local studies. Here, we use ranges of diffusivity provided in recent works pointing to a higher importance of mountain block recharge than previously assumed. We consider diffusivity values of 0.1, 0.3, and 0.5 m^2/s for Sierra's crystalline fractured rocks. We also consider depths within a range of 600-1300 m for vertical distance from the high mountains to the deep aquifer layers below the Corcoran clay.

https://doi.org/10.5194/egusphere-2024-4023
Preprint. Discussion started: 19 March 2025

We solve the parabolic differential Equation 4 using the function *pdepe*() from the Matlab software by setting the initial pressure conditions to zero and the boundary conditions of the pore-fluid pressure at the top of the aquifer to a periodic variation with periodicity ψ of 1 year, annual amplitude P_{max} and annual phase φ_0:

$$P'_{z,t=0} = P_{max} \cdot \cos\left(\frac{2\pi}{\psi} t + \varphi_0\right) \quad (5)$$

where at depth z, pore-fluid pressure is $P_{z,t} = P_{z,t-1} + P'_{z,t}$. We are only interested in changes $P'_{z,t}$ of pore-fluid pressure. We do not introduce a boundary condition at the bottom of the aquifer.

Assuming saturated conditions and solving Equations 4 and 5 for t allows us to estimate the time it takes to increase pore-fluid pressure annually due to groundwater recharge reaching vertically from top groundwater layers to depth. The duration of pressure propagation to deep aquifer layers is independent of the amplitude of pressure change at the surface and a normalized solution for $P'_{z,t=0}/P_{max}$ is sufficient. The time delay estimate is most sensitive to the magnitude of the hydraulic diffusivity κ (Eq. 4) as well as the phase φ_0, of the annual pressure variation due to recharge (Eq. 5). We further assume that the horizontal diffusivity of the aquifer is large enough, and despite the width of the valley and hydrological complexities, it is likely that the lateral diffusion rate is relatively small, compared to the vertical diffusion rate (Fetter & Kreamer, 2022).

The annual phase of pressure variations in upper groundwater layers in the high Sierra Nevada φ_0 may be derived from the annual variation in water available for recharge in this region, which we quantify as follows. Here, we refer to the upper parts of the mountain block connected to the water supply from the surface, which experiences increased water pressure during the rainy and melting seasons without much time delay. Hence, these top groundwater layers in the Sierra Nevada receive inflow from snow melt water and liquid precipitation (i.e., rainfall). Urióstegui et al. (2017) and Bales et al. (2011) found that only 10-20% of the snow melt water in the Sierras runs off through streams, with the remainder being lost to drainage into deep layers and evapotranspiration. We assume that all of the melt water initially increases pressure in the upper groundwater layers of the Sierra Nevada before evaporating or running off. Also, we neglect the delay between the time that water for infiltration becomes available and its percolation into the upper groundwater layers of the Sierra Nevada. We consider these assumptions reasonable for wide areas of exposed fractured bedrock, given that we are only interested in quantifying the phase and not the absolute value of maximum pressure variations. For that, we retrieve the time series of SNODAS dataset variables 'snowmelt runoff at the base of the snowpack' M and 'liquid precipitation.' P_{liqu} (see Section 2.1, Fig. S1) averaged for the drainage area of the Sierra Nevada toward the CV (rose-shaded area in Fig. 1a). We correct liquid precipitation for canopy interception by a relative value of 20%, adapting this estimate from previous studies for mixed forests in the Sierra Nevada (Bales et al., 2011). This intercept changes the relative amplitudes between M and P_{liqu}, and therefore, it can impact the annual phase. Finally, we get a time series of total water available for recharge in the Sierra Nevada drainage area from ($P_{liqu} - 0.2 \cdot P_{liqu} + M$) and quantify monthly mean values of this time series during 2002-2020 (Fig. S2c). We also determine the mean timing of the annual peak for each year and at each location in the drainage area, which we apply as the timing of the annual maximum of the pressure variation to constrain φ_0 for the boundary condition in Equation (5).

4 Results

4.1. Year-to-Year Water Variability

The time series of TWS variations obtained from the GRACE satellites (Tapley et al., 2004, 2019) and their components measured through in-situ observations (e.g., wells) (Alam et al., 2021) or water balance models (Faunt, 2009; Li et al., 2018) are characterized by annual variations attributed to overall dynamics in the terrestrial water cycle (Tang & Oki, 2016). Several example time series are shown in Figure 1c. A less obvious pattern comprises the interannual variations in the amplitude of the annual signal. Identifying the amplitude and timing of the peak annual and interannual signal components allows for resolving the temporal scale at which the connected systems interact.

To this end, we apply the wavelet-based time-frequency analysis to extract hidden patterns in the datasets (see Section 2.2.1, Fig. S6). The results from the time-frequency analysis are shown in the form of a PSM, distributing the signal's power into frequencies (or periods) and time intervals (Fig. 3, S7). We find maximum amplitudes characterize the PSMs associated with different time series at equivalent periods of 1 year and 3-8 years (Fig. 3). These frequency components are associated with general variations in water availability associated with atmosphere-ocean interactions, influencing water cycles in the Southwest USA (Quiring & Goodrich, 2008). Significant drought periods, such as during 2007-2009 and 2012-2015 (Fig. S3), correspond with cool phases of El Niño Southern Oscillation (ENSO) recurring every 3-7 years, the cool phase of the Pacific Decadal Oscillation (PDO), and the warm phase of the Atlantic Multidecadal Oscillation (AMO) (McCabe et al., 2004; Quiring & Goodrich, 2008). The length of our observation does not allow for resolving signal components over a decade or longer, as indicated by the cone of influence, the shaded region in the PSM.

Some PSMs also show unique patterns. For instance, the PSMs of GWL changes (Fig. 3a) and GNSS VLM (Fig. 3b) exhibit components at periods of 0.5 and 3 years, albeit the component of 0.5 years for VLM disappears following 2008. In contrast, the PSM of SnS (Fig. 3e) shows only a transient component over 3 years. PSM of GWS variations (Fig. 3g) shows a transient component of 1 year period. Notably, the location and amplitude of peak PSM are not constant and change over time, especially for TWS, SnS, ReS, and GWS variations and to a lesser extent in SoS due to water availability changes within wet and dry seasons and in between them as well as due to human interventions. For instance, the amplitude of annual components was reduced or diminished during the drought years 2007-2010 and 2012-2015. During these periods, reservoirs were not refilled, and the Sierra Nevada received little precipitation, reducing the amplitude of the corresponding annual components (Fig. 3e and 3f). The amplitude of the annual component of GWS variations vanishes during the same years (Fig. 3g).

https://doi.org/10.5194/egusphere-2024-4023
Preprint. Discussion started: 19 March 2025

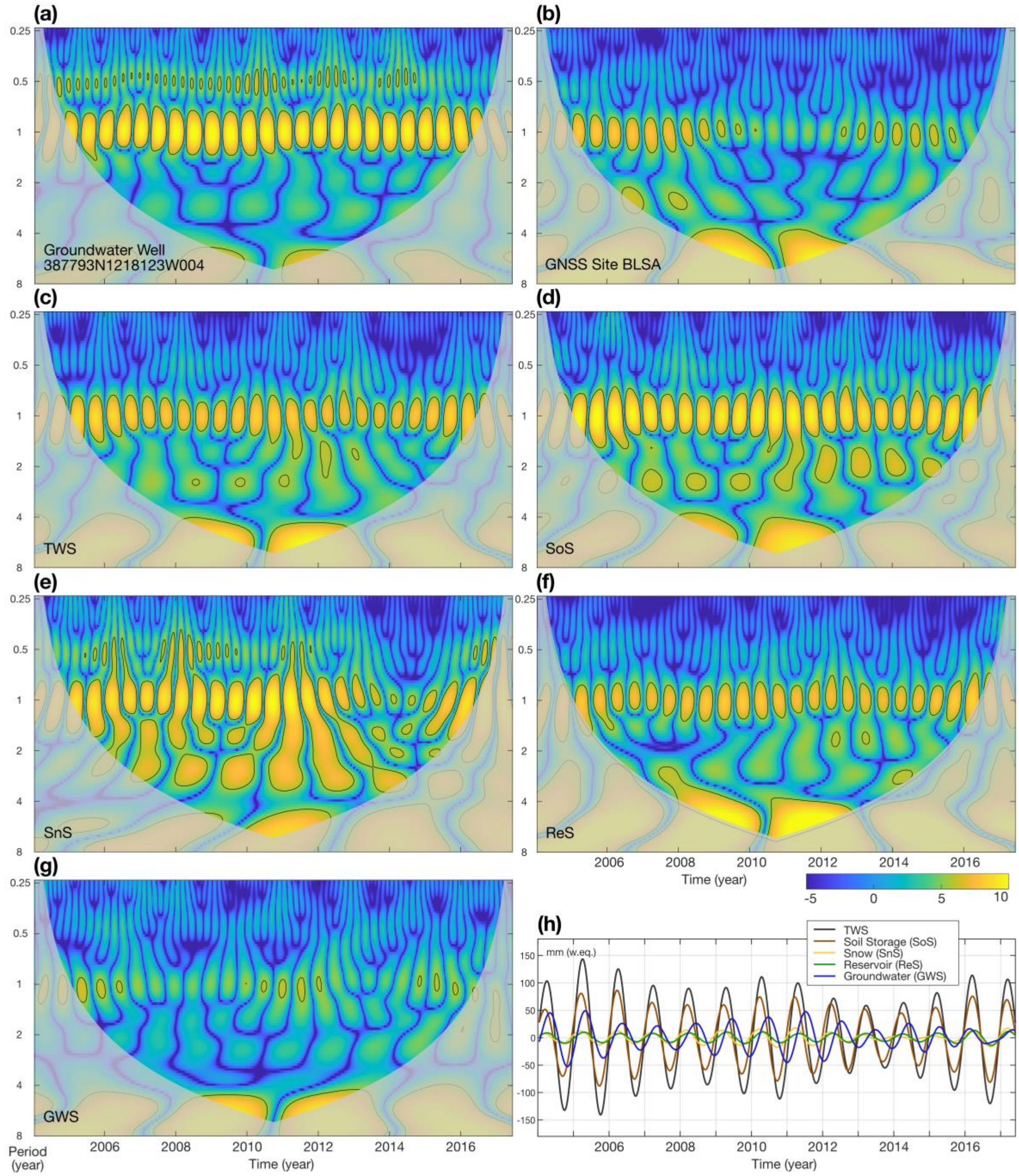

Figure 3. Wavelet time-frequency analysis. A wavelet analysis was performed for time series of all available datasets to isolate the annual signal component. Wavelet spectrum of time series of (a) groundwater level at well 387793N1218123W004 and (b) vertical land motion at GNSS site BLSA (see Fig. 1 for their location), and of average water storage variations in the GRACE region: (c) total water storage (TWS) from GRACE, (d) soil storage (SoS) from GLDAS and WGHM, (e) snow storage (SnS) from SNODAS, (f) reservoir storage (ReS) from CDWR and (g) groundwater storage (GWS) in CV. (h) Reconstructed annual signal component for periods within range of 0.75-0.25 years from water storage wavelet spectra shown in panel c-g.

https://doi.org/10.5194/egusphere-2024-4023
Preprint. Discussion started: 19 March 2025

Figure 3h presents the isolated annual components for all the time series comprising PSM components of 0.75 to 1.25 yr periods, which display non-stationary behaviors, i.e., the amplitude changes over time. We find that year-to-year TWS is experiencing the most pronounced changes and GWS the least. We also note that year-to-year peak extremes do not co-occur for different time series. For instance, during the 2012-2015 drought, TWS, SoS, and ReS variations experienced their lowest amplitudes in 2013 and 2014, while that of GWS occurred two years later during 2016, following the snow-poor years in 2014 and 2015. Characterizing such inter-annual variability in water cycle components improves understanding of the region's hydroclimate extremes and water storage capacity (Yin & Roderick, 2020).

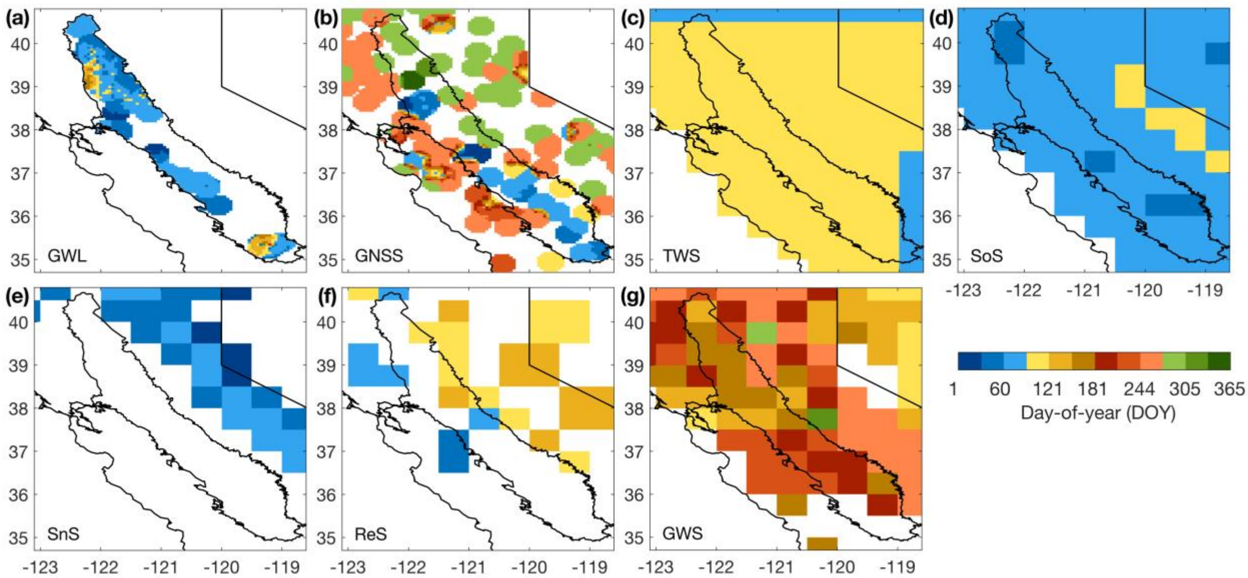

Figure 4. Timing of annual maximum of groundwater related signals. Timings are given in day-of-year (DOY). (a) Groundwater levels (GWL) at 250 observation sites throughout the Central Valley providing at least three years of data during 2002-2020 at depths below 50 m. (b) Vertical land motion (maximum uplift) at 170 GNSS sites throughout entire California with a seasonal amplitude larger than the median of the time series error standard deviation. Timing for groundwater and GNSS were inversely interpolated using a 25 km correlation radius. Remaining panels show timing of annual maximum water storage at 0.5-degree sampling resolution: (c) total water storage (TWS) from GRACE, (d) soil storage (SoS) from GLDAS-Noah, (e) snow storage (SnS) from SNODAS, (f) reservoir storage (ReS) from CDWR and (g) resulting groundwater storage (GWS). White areas have either no data or amplitude of annual variation is near zero. Annual oscillations of vertical land motion inside the CV are temporally aligned with those of groundwater level variations. In contrast, oscillations of vertical land motion outside the Central Valley are in resonance with annual oscillations of total water storage changes detected by GRACE (compare panel b with c, and Fig. 6), because maximum VLM outside the Valley is driven by minimum elastic load of the water masses. Individual values for groundwater well and GNSS sites, timing of minima, related histograms, and standard deviations of annual timing during observation periods are shown in Figures S8, S9, S10, and S11.

https://doi.org/10.5194/egusphere-2024-4023
Preprint. Discussion started: 19 March 2025

4.2. Timing of the Seasonal Signal

We further investigate the spatial variability of the timing of the peak annual amplitude of TWS and its components across the study region (Fig. 4). Note that spatial detail cannot be resolved from the GRACE TWS with 300-400 km spatial resolution. To this end, we find the day-of-year (DOY) corresponding with the peak of the time series of the annual components and then obtain the median of DOY for each time series. Figure 4 plots the median peak DOY for each dataset at their original spatial resolution, except for GWL and VLM, where the values are interpolated with an inverse distance weighting scheme with a 25 km radius. The median peak DOY for GWL is uniform across the Valley (Fig. 4a, S8) with negligible interannual variability (Fig. S9). GWL peaks occur from February to March (Fig. 4a, S8a) and minima in August (Fig. S8b). The fastest GWL rate increase (i.e., the mid-point between annual minima and maxima) occurs during November (Fig. S8c), and the fastest GWL rate decrease (i.e., the mid-point between annual maxima and minima) occurs during May (Fig. S8d). These observations are consistent with the timing of maximum pumping in the CV from April to June. A linear correlation of 0.3 was found between observation well depth and peak DOY, indicating GWL rises slightly later in the year at deeper wells (Fig. S8a, left inset). Compared with GWL, the median peak DOY of GNSS VLM in the CV is spatially more variable (Fig. 4b and S10), with negligible interannual variability (Fig. S11). We find a bimodal distribution for this peak DOY (inset in Fig. S10a), with about a third of the stations within the CV peaking from March to April and most of the remaining stations from September to October. A bimodal behavior is also observed in the median DOY of annual VLM minima. The median DOY of the fastest VLM rate increases and decreases are also obtained (Fig. S10), indicating a smaller interannual variability than that of peak DOY (Fig. S11). We further estimate the median peak DOY of TWS, SoS, SnS, ReS, and GWS within the GRACE region (Fig. 1b), all of which show spatially uniform patterns but are distinct from each other (Fig. 4c-g), with spatial DOY averages of 93, 70, 65,102, and 156 days, respectively.

We performed a similar analysis using InSAR LOS deformation observations. Figure 5a shows the LOS velocity field measuring up to 18.5 cm/yr subsidence in some parts of San Joaquin Valley. We obtained seasonal phase (peak DOY) and amplitude (Fig. 5b, c) for the southern CV covered by the Sentinel-1 frame. The spatial distribution of median peak DOY generally agrees with that of GNSS (Fig. 4b). The denser spatial sampling from the InSAR analysis, however, reveals a more detailed pattern for the propagation of the deformation. With some exceptions, we find a main feature indicating an outward propagation of the median annual peak DOY from the center of the San Joaquin Valley, especially in areas where the Corcoran clay sits deeper (compare Fig. 1a), towards the sides of the valley where the Corcoran clay sits shallower. Although it varies yearly, the overall outward propagating pattern of peak DOY remains similar through wet and dry years (Fig. S15), while amplitudes are lower in the dryer years (e.g., 2018). We note that this result seemingly contradicts what Neely et al. (2021, 2024) found, who suggested an MFR-driven inward propagation of the annual peak towards the center. We address this further in the discussion section below. Figures 5c and S16 show the median and yearly seasonal amplitude of surface LOS deformation, reaching up to 4 cm, with the largest value during dry years.

https://doi.org/10.5194/egusphere-2024-4023
Preprint. Discussion started: 19 March 2025

Next, we investigate the empirical probability density function (PDF) of annual peak DOY associated with all components of TWS and deformation and several other relevant hydrological datasets (Fig. 6). Shown are normalized PDFs of annual peak DOY obtained for each year and each time series without temporal averaging, thus the interannual variabilities are preserved. Comparing different PDFs, we find for the Sierra Nevada that precipitation generally peaks in early January, with a mean DOY of 16 (Fig. 6a), meltwater in late February, DOY 55 (Fig. 6c), and the total water availability (combination of precipitation, meltwater, and canopy interception) in late January, DOY 22 (Fig. 6b). We obtain a wide distribution for the influxes, and years with a later maximum melt typically have a larger peak, causing the right-skewed distribution of annual peak DOY of snowmelt (Fig. S2b). The annual SoS peak for the CV occurs in March, DOY 70 (Fig. 6d), ~2-3 months after precipitation peaks. SnS peaks in March, ReS and TWS ~1 month later in April, while GWS of the CV peaks in June (Fig. 6e-g). The VLM minima (i.e., subsidence) across California, outside of the CV, co-occur with TWS maxima around April, DOY 93 (Fig. 6i). In contrast, GNSS VLM inside the CV (Fig. 6j) peaks together with GWL (Fig. 6k) around March, DOY 65, and ~3 months before GWS based on GRACE and composite hydrology (Fig. 6g). Peak VLM inside the CV derived from high-resolution InSAR maps (Fig. 6k, dashed line) have a more complex distribution, with the first peak co-occurring with GNSS and well levels around the beginning of March and a later peak ranging from beginning to end of April. We further observe a delay of 43 days between the total water available for recharge in the Sierra Nevada Drainage area (DOY 22, Fig. 6b) and GWL in the CV (DOY 65, Fig. 6k).

To investigate whether the mean values of the PDFs in Figure 6 were significantly different, we performed a two-sample mean difference hypothesis test using the t-distribution (Meyer, 1970). We formulated the null hypothesis so that the mean values were the same and tested the hypothesis at a significance level of 0.05. The test was rejected, hence, the mean values are statistically different for all pairs of PDFs in Figure 6, except between GNSS uplift (CV) and GWL (CV), between TWS and GNSS Subsidence (CA), between SnS (Sierra Nevada) and GNSS uplift (CV), and between SnS (Sierra Nevada) and GWL (CV).

When estimating PDFs for the timing of annual peaks of SoS and GWS (Fig. 6e and 6g), the variability among the individual SoS models was considered (Fig. S12). SoS timing varies by about ~2 months from January to February (Fig. S12c). We propagate the variation of SoS timing toward that of GWS by estimating GWS for each individual soil model (Fig. S13a). The resulting annual GWS timing varies ~2 months from May to July (Fig. S13b,c). This variability was included when calculating mean, median, standard deviation, and PDFs of annual GWS timing (Fig. 6g). Although GWS also depends on the timing of TWS, SnS and ReS, annual amplitudes of SnS and ReS are only 10% of TWS (Fig. 1c). Therefore, they will only marginally impact the calculation of annual timing of GWS. We assume a minimal measurement uncertainty for the timing of TWS.

https://doi.org/10.5194/egusphere-2024-4023
Preprint. Discussion started: 19 March 2025

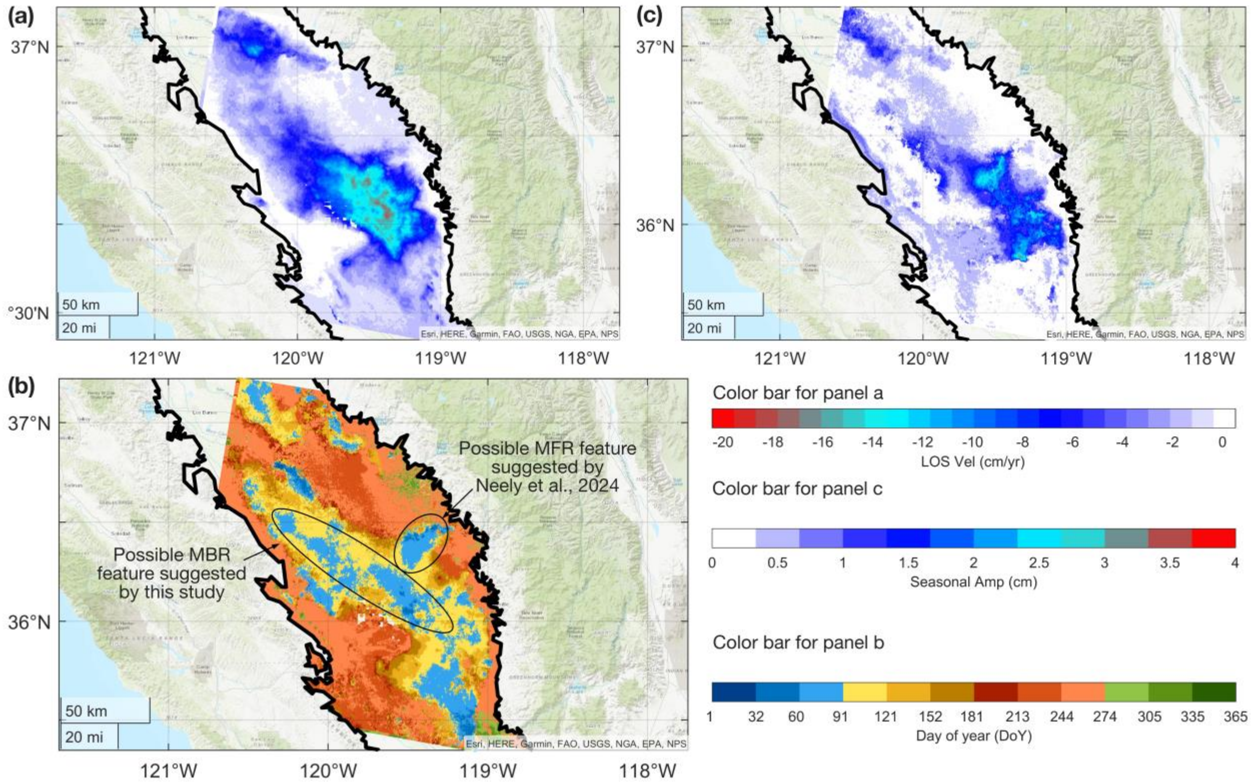

Figure 5. a) LOS velocity map for the period 2015/11/27-2022/12/20. b) Median seasonal phase (peak DOY) highlighting suggested features caused by Mountain Block Recharge (MBR) and Mountain Front Recharge (MFR), and (c) amplitude of InSAR deformation time series for water years 2016-2022. See Figs. S15 and S16 for yearly phase and amplitude maps, respectively.

4.3. Pressure Diffusion from the High Mountains to Deep Valley Aquifers

Assuming an existing hydraulic connection between deep CV and High Sierra Nevada mountain aquifers through the fractures in the mountain block, as conceptualized in Figure 2, it takes some time for the water pressure to reach depth. We provide a first-order estimate for the diffusion time, the time it takes for a seasonal pressure front to vertically diffuse from the top aquifer layers in the Sierra Nevada down to elevations of the deep CV aquifers (Section 2.5, Eq. 4). If we quantify that using a hydraulic diffusivity $\kappa = 0.3$ m^2/s for the Sierra's crystalline fractured rocks, it takes 18-36 days for the pressure to travel vertically to depths of 600-1300 m (Fig. 7). Delay times for all depths at 100m increments are visualized in Figure 7 and example numerical values are provided in a table inset therein. We further consider a range for the vertical hydraulic conductivity and evaluate the diffusion time for $\kappa = 0.1$ m^2/s and $\kappa = 0.5$ m^2/s to a depth of 600-1300 m, corresponding with 34-73 days and 12-23 days (Fig. S14), respectively.

https://doi.org/10.5194/egusphere-2024-4023
Preprint. Discussion started: 19 March 2025

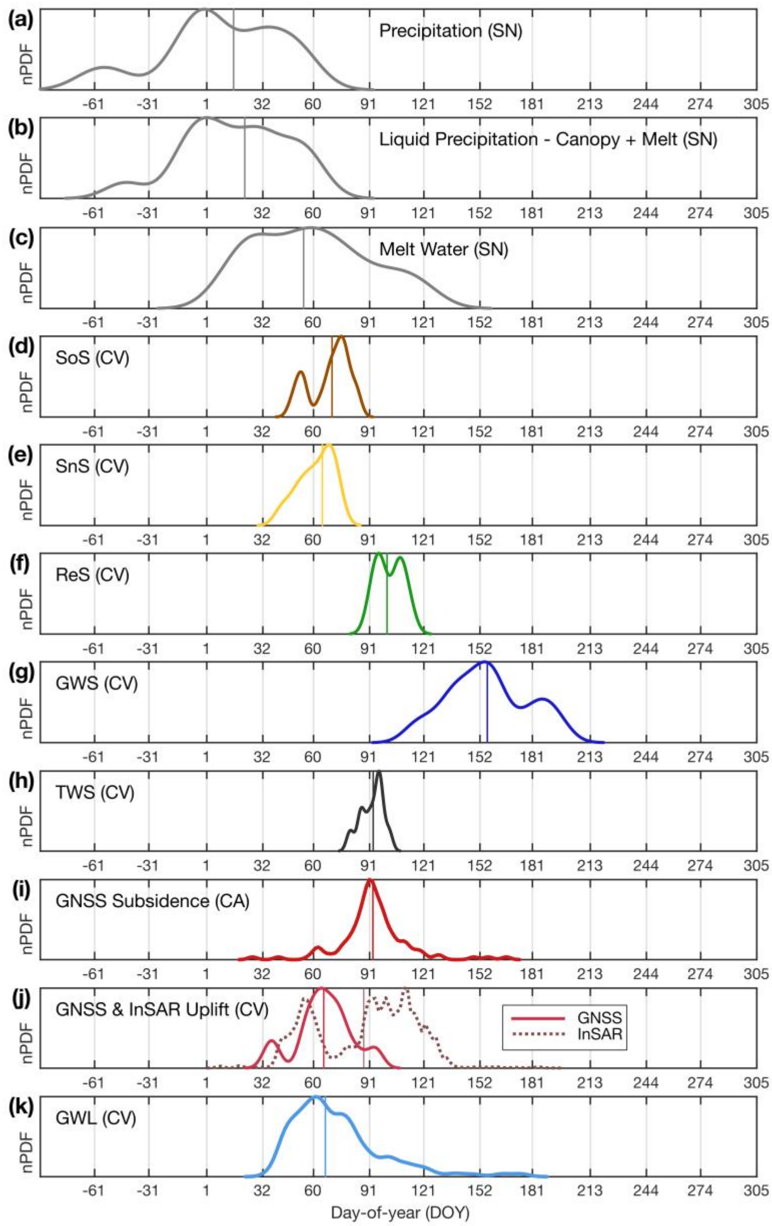

Figure 6. Normalized probability density functions for timing of annual extremes in groundwater-related signals across California. Row and line color indicate signal type: (a) total precipitation in the recharge area of the Sierra Nevada (SN, see Fig. 1a) from SNODAS, (b) Sum of liquid precipitation and melt water corrected for canopy interception in SN from SNODAS, (c) Melt water in SN from SNODAS, (d) soil storage from hydrological models for GRACE region corresponding with the Central Valley (CV, Fig. 1b), (e) snow storage from SNODAS for CV, (f) surface reservoir storage from CDWR for CV, (g) GRACE-based estimate of groundwater storage for CV, (H) total water storage from GRACE for CV, (i) vertical land motion from GNSS for all available sites in California (CA), and (j) for GNSS sites (red) in the CV only, and for InSAR pixels in the southern CV from Fig. 5 with a seasonal amplitude larger than 3 mm, and lastly, (k) groundwater levels from observation wells in CV. See Figure 1 for the location of subregions. Each function indicates the maximum probability for the timing of the annual maximum (a-i, k) or minimum (j) amplitude of the annual signal based on wavelet analysis (Fig. 3 and Fig. S7). Vertical lines represent the mean value for the timing of annual maximum. Distribution is normalized by maximum probability density value and results from year-to-year variation of the regionally averaged gridded datasets (a-h) and from spatial variation of well and GNSS data sets (i-k).

https://doi.org/10.5194/egusphere-2024-4023
Preprint. Discussion started: 19 March 2025

5 Discussions and Conclusions

This study performs time-frequency analyses of large hydrologic and geodetic datasets across California with various spatiotemporal resolutions and uncertainties to characterize the annual peak DOY, interannual peak amplitude variations, and correlative behaviors across these observations. We observe relatively low seasonal peaks during droughts for all components of water storage (Fig. 3h). However, only for storages in snow and groundwater wavelet PSMs vanish completely at periods of around one year during droughts when snow cover was diminished to absent during 2007 and 2012-2015 (Fig. 1c, 3e, 3g). We interpret this correlation as an indicator that the volume of the snowpack and the following snowmelt plays a substantial role in groundwater recharge in the CV. Once corrected for SoS, SnS, and ReS, GRACE measures a combination of GWS change in shallow and deep aquifers. Hence, we consider snow relevant for both MFR and MBR, with the former mechanism being more relevant for replenishing the shallow and the latter for (slow) flow to the deep aquifers, given the depth of their flow path.

We further observe that GNSS VLM and InSAR LOS peak DOY vary across California. The peaks for stations inside the CV co-occur with that of GWL (Fig. 6j, k), specifically at the sites near the center of the Valley, where aquifer confining layers are thick and observed annual amplitudes are large (Fig. 5). This indicates the presence of poroelastic aquifer deformation due to groundwater pumping (Ojha et al., 2018; Smith et al., 2017). In contrast, the VLM peak minima for stations outside the Valley co-occur with that of TWS peak maxima (Fig. 6h, i), attributed to the variations in elastic water loading (Argus et al., 2017; Carlson et al., 2022; Johnson et al., 2017). Interannual variability in the peak amplitudes impacts the hydroclimate trends, changing baselines used to assess the future risk of climate extremes and vulnerability of water resources (Stevenson et al., 2022). In summary, a similar peak DOY suggests that some components of the hydrological system act in concert with or respond elastically to similar hydroclimate forcing or anthropogenic factors. In contrast, a different peak DOY may indicate a cascading nature of the response to forcing governed by a time-dependent process.

Following recent local hydrological and hydrochemical studies (Armengol et al., 2024; Schreiner-McGraw & Ajami, 2022), we propose that MBR through the fractured granite of the mountain block is an important process, allowing long-term recharge to deep aquifers in the CV, and we further suggest that MBR occurs at the regional scale. Earlier studies (e.g., Gilbert and Maxwell (2017)) have suggested that such a natural connection between deep CV and High Sierra Nevada mountain aquifers should exist. Studies that examined long-term trends in precipitation and groundwater level records (e.g., (Gardner & Heilweil, 2009; Kuss & Gurdak, 2014)) suggested a delay of 2-25 years in groundwater level responses across the U.S., however, these studies do not investigate the short-term interactions. The feasibility of this mechanism at short time scales is demonstrated in Fig. 7, where a first-order process-based pressure diffusion model quantifies the lag between peak pore pressure in the Sierra Nevada aquifers due to snowmelt and peak pore pressure within deep CV aquifer layers. We estimate the lag at about a month, ignoring the lateral diffusion time, which is often negligible for permeable aquifers such as CV (Fetter & Kreamer, 2022). Given the uncertainty range of hydraulic diffusivity (Somers & McKenzie, 2020), the estimated diffusion time agrees well with the observed lag between peak water availability in the mountains and peak GWL

https://doi.org/10.5194/egusphere-2024-4023
Preprint. Discussion started: 19 March 2025

in deep aquifers (Fig. 6b and k). This agreement supports the hypothesis that high mountain aquifers are connected to deep valley aquifers through pressure propagation from MBR, and that it drives seasonal well level changes in the deep CV aquifers.

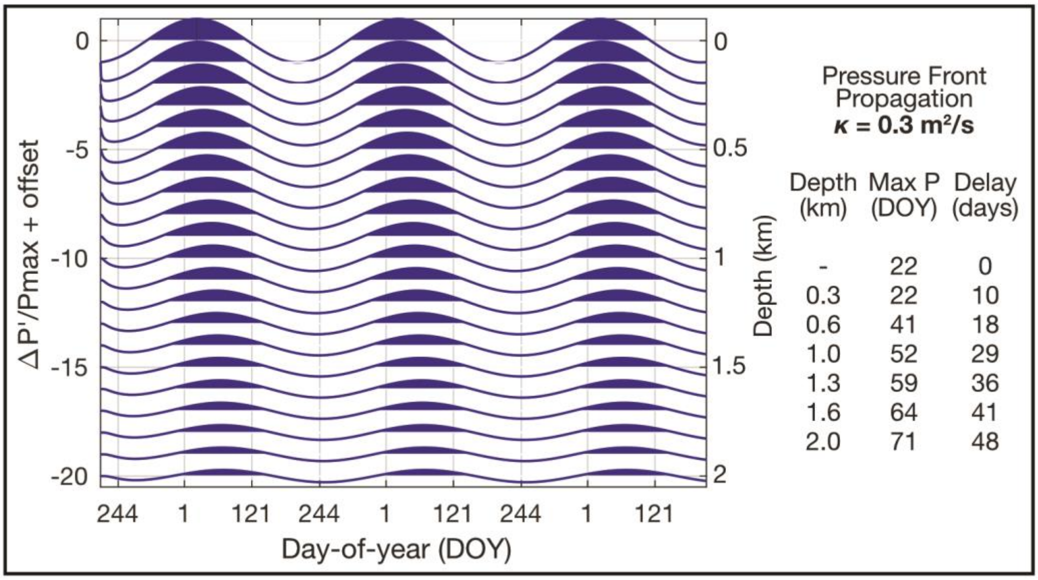

Figure 7. Vertical pressure propagation for elevation difference between the Sierra Nevada and the Central Valley aquifers. Normalized pressure change ($\Delta P'/P_{max}$) at different depths due to standard 1D calculation of pressure front propagation along mountain block recharge conduits in the fractured bedrock of the Sierra Nevada. Graphs are incrementally offset by -1 for each depth. In top groundwater layers, maximum pressure occurs on January 22nd (DOY 22), which is driven by mean annual water availability in the recharge area (Fig. 6b). Table to the right indicates DOY and time delay of the pressure propagation to a depth of 300-2000 m. Given a hydraulic diffusivity κ = 0.3 m^2/s (reasonable for fractured granite bedrocks), the pressure front needs ~0.6 (1.2, 1.6) months to propagate to a depth of 600 (1300, 2000) m. A smaller hydraulic diffusivity would lead to a slower propagation to depth and vice versa, examples for κ = 0.5, 0.1 m^2/s are shown in Figure S14.

A hydraulic connection between surface and deep aquifers cannot explain the annual increase in deep wells below the Corcoran clay. Pumping from the deep, confined aquifers can only explain the annual decline in groundwater levels. Hence, the diffusivity of the system must be high enough to allow pressure propagation at seasonal scales.

We also tested the assumption of a negligible horizontal flow by applying the propagation model for an additional horizontal flow of 10 km through horizontal layers of diffusivities within a range of 10 m^2/s to 80 m^2/s and estimated that the additional diffusion time is 18 to 51 days. This added time delay is still consistent with the range of uncertainties for the observed delay between maximum water availability in the mountains and maximum groundwater levels in the valley (see Fig. 6b&k) as well as within the considered range for tested hydraulic diffusivities (Fig. S14).

The peak GWL in March likely occurs earlier than it would naturally due to anthropogenic influence since heavy groundwater pumping onset typically occurs in April and May. Consequently, the observed delay time might be underestimated, and a naturally occurring later GWL peak would suggest a longer vertical diffusion time. This, however, is

https://doi.org/10.5194/egusphere-2024-4023
Preprint. Discussion started: 19 March 2025

consistent with the considered range for tested hydraulic diffusivities (Fig. S14). Even though we rely only on observation wells, we likely cannot completely isolate the natural recharge from the pumping signal with the presented data analysis. We want to note that pumping induced faster GWL decline in deep CV aquifers further increases the pressure gradient toward the high mountains, which could intensify the pressure propagation along MBR flow paths. In addition, the unusual late timing of maximum GWS based on GRACE estimates compared to the timing of maximum GWL, one of the main findings of this work, is likely not affected by pumping because it would affect both signals equally.

Here, we do not consider the impact of poroelastic stresses on pore pressure propagation due to surface loading (e.g., due to changes in reservoir storage). This contribution is negligible for unconfined aquifers due to their relatively small Skempton coefficient (Wang, 2000). However, it is slightly larger for (semi-)confined aquifers, though still orders of magnitude smaller than that of pore pressure change (see, for instance, Zhai et al., 2019).

We further observe an outward migration of the InSAR LOS peak DOY from the center of the CV (Figs. 5b and S15). This pattern occurs throughout the entire San Joaquin Valley, with a few exceptions. This finding seems at odds with the previously published works (e.g., Neely et al., 2021, 2024) that suggested an inward propagation of annual peak DOY from the Sierra Nevada toward the center of the CV. However, their interpretation relates to local patterns near the mountains in the deformation maps, for example, arrow-shaped feature in the northeastern section of the map, which is also visible in our results (compare the marked feature in Fig. 5b with their Figure 4a, near latitude 36.5°N and longitude 119.25°W). They suggested that MFR fed by surface water flowing off the Sierra Nevada may replenish aquifers (deep and shallow) seasonally across the southern CV (Neely et al., 2021, 2024). While we agree that these local patterns are a good indication of recharge near the front of the mountain, they do not explain the entire widespread early peak in the center of the valley with outward migration in most surrounding areas, e.g. northwest and south of the mentioned feature. The deformation signal is a vertically integrated signal for the entire CV aquifer system; hence, it is expected that it shows dynamics due to both mechanisms, which also may overlap in some areas. We further think both mechanisms must be at play because the MFR mechanism is implausible to solely recharge deep confined aquifers (Shirzaei et al., 2019) due to the presence of the impermeable Corcoran clay layer and widespread clay lenses (Faunt, 2009). These lenses reach toward the front of the mountain, as recently visualized by Neely et al. (2024) via electromagnetic resistivity observations (Fig. 6 therein), and the suggested MFR pathways by the authors do not reach depths below the Corcoran clay. In addition, there is little evidence of widespread vertical cracks and deep extensional fissures in the Valley (Carlson, Shirzaei, Ojha, et al., 2020) to provide a potential pathway for water to percolate deep into the aquifers, though further research on extensional cracking and fissure initiation in the Valley is needed (Carlson, Shirzaei, Ojha, et al., 2020). In contrast, our hypothesis of MBR linking Sierra groundwater to deep CV aquifers is consistent with Darcy's fluid flow law, linking the fluid discharge rate to the hydraulic head gradient between two given points, scaled with the hydraulic conductivity, which is related to diffusivity through the inverse of the specific storage. Under constant hydraulic conductivity, flux (q) is proportional to head gradient (dh/dl); namely, $q \propto dh/dl$. Thus, the largest flux recovery happens to the point of the largest head gradient. In the CV, it is logical to assume that the largest gradient and zone of the fastest subsidence rate is where the heads are lowest, consistent with

https://doi.org/10.5194/egusphere-2024-4023
Preprint. Discussion started: 19 March 2025

groundwater level observation. Thus, the pressure propagation from the Sierra Nevada could recover aquifer pressure near the center of the Valley first and then propagate outward from the center to areas with smaller hydraulic gradients, as observed here. Hence, we interpret the InSAR LOS observation of annual peak DOY as additional support for the hypothesis of a direct pressure link between the Sierra Nevada aquifers and CV deep aquifers through mountain block conduits.

An unexpected finding is the phase difference between annual peaks of GWL in deep confined aquifers and GWS in the entire CV aquifer system (including confined and unconfined units, Fig. 4a, 4g, 6g, and 6k), which is about three months. This indicates that different processes influence GWS and well levels. In confined units, the well level change is driven by changes in groundwater storage and pore fluid pressure, while the gravity-derived measurements only detect the change in mass, hence, storage changes. During the spring, pressure rises faster in the deep aquifers than storage is recovered therein. A vertical hydraulic connection via MBR flow paths would allow pressure change propagation from the mountain to CV aquifers at seasonal time scales. However, direct water seepage along MBR flow paths takes longer (Berghuijs et al., 2022). The proposed mechanism here does not require immediate water percolation. It is consistent with the tracer findings that deep groundwater in the CV is primarily old (McMahon et al., 2011), although, a smaller portion of the seasonal storage available in the mountains might still propagate to the deep aquifers along MBR flow paths. Our results further emphasize that vertical pressure propagation occurs faster than net recharge (i.e., detected as storage change) from the mountain aquifers to the valley aquifers. The later peak in GWS might be primarily driven by annual storage variations in top unconfined aquifer layers (Vasco et al., 2022), which would recharge faster than deep aquifers. This is also consistent with the relatively late mean annual peak in meltwater occurring during early May (see Fig. S2), hence, a long-lasting supply for recharge through surface-groundwater links along the mountain fronts until late spring. At annual time scales, MFR likely contributes a significant portion to storage changes in shallow aquifers, and the seasonal variation in GRACE GWS mainly comprises such shallow aquifers instead of deep aquifers. From these observations, we conclude that the seasonal well level rise in deep CV aquifer layers may be driven dominantly by pressure rather than storage variability. During the melting season, storage increases in the mountain aquifers. However, this seasonal storage increase might be temporary, driving the seasonal pressure increase in the valley, but dissipating to other flow paths before passing water volume to the deep CV aquifers. This is feasible when considering the deep CV and the high mountain aquifers as two separate aquifer systems connected through shallow MFR and deep MBR flow paths, as conceptualized in Figure 2.

It should also be noted that the MBR estimates based on GNSS and GRACE constraints from Argus et al. (2022) were derived as the difference between gravity and elastic loading-based annual GWS estimates to the output of a hydrological model, not including MSR. The authors interpret this difference solely as MBR and neglect the contribution of MFR in the estimate because the method they apply cannot discriminate between the two MSR processes. To reliably quantify MBR at the scale of the CV and discriminate it from MFR, we suggest the implementation of a fully fluid-solid media coupled 3D groundwater model for the CV that integrates the wealth of hydrologic and remote sensing observations sensitive to the dynamics in the aquifers as demonstrated in this study. The results should also be crosschecked with observations of groundwater ages, e.g. based on isotope studies (Earman et al., 2006).

https://doi.org/10.5194/egusphere-2024-4023
Preprint. Discussion started: 19 March 2025

Our study uses a data-driven approach that does not include detailed physical process simulations. The 1D-pressure propagation model ought to demonstrate the general feasibility of the MBR via a hydraulic connection from the Sierra Nevada to the deep Central Valley aquifers, and we think it is well supported by the hydrological and geodetic observations we presented. To further quantify and prove this link, we emphasize the need for future regional studies that implement physics-based models accounting for groundwater flow (Schreiner-McGraw & Ajami, 2022) and isogeochemical characterizations (Armengol et al., 2024) as mentioned above. Detailed model experiments will also help to determine of the human impact, i.e., via pumping and managed aquifer recharge, on the various aquifer recharge fluxes, which we cannot specify with the presented observations alone.

Our findings are subject to uncertainties, albeit statistical tests of significance help corroborate the main results. The wavelet time-frequency analysis is affected by data gaps and variable sampling rates, similar to other spectral methods (Goswami & Chan, 1999), although the ability of the continuous wavelet transform to localize signal components in time and space minimizes error propagation. GNSS sites may be affected by other processes causing annual oscillations, such as non-tidal loading, tectonic processes, thermoelastic deformation, and draconitic errors (Chanard et al., 2020). Errors in the GWS component from GRACE observations are subject to any error in the correction terms, which propagates into the GWS time series. However, the three-month delay between the peak of GWS and GWL remains robust against the uncertainty in the timing of GWS (see Section 4.2). Hence, the measure that pressure propagates faster to deep aquifer layers than the groundwater volume change in the entire aquifer remains unaffected. The total number of 22 deep aquifer well sites available in the south is relatively low. However, in our analysis, we prioritized data reliability over quantity. We chose a lesser number of observation wells to ensure that they are less affected by the pumping signal and to provide data from semi-confined to confined layers. We believe this serves to ensure the accuracy of our findings regarding the timing of the annual maximum groundwater level and, therefore, the significance of our conclusions. Lastly, the diffusivity parameter applied in the 1D poroelastic model has a large uncertainty range because little is known about the actual extent and depth of fractures in the crystalline bedrock. Recent studies support comparable large diffusivity values as we applied here, especially at the regional scales where secondary porosity becomes effective (see above). However, the parameter should be further validated for the region via careful hydrological model experiments, ideally assimilating a variety of hydrological and geodetic observations. Also, more detailed textural information about the mountain block is needed to quantify diffusivity more accurately at large scales, which could be acquired by extensive or innovative field campaigns (Viswanathan et al., 2022).

Driven by changing climate, the intensity and frequency of extreme climate events are projected to increase throughout the 21st century (AghaKouchak et al., 2020), and they likely impact groundwater availability by modifying the recharge and discharge processes (Meixner et al., 2015; Taylor, 2012). For instance, Siirila-Woodburn et al. (2023) suggest that years with atmospheric rivers result in lower aquifer recharge. However, we do not consider the effect of climate extremes in our analysis because their overall impact on groundwater recharge is unclear due to the lack of mesoscale models integrating General Circulation Models (CGMs) under different emission scenarios with hydrological models (Smerdon, 2017).

Recent studies (Ajami et al., 2011; Markovich et al., 2019; Meixner et al., 2016; Somers & McKenzie, 2020; Wahi et al., 2008; Welch & Allen, 2014) have recognized mountains' critical role in freshwater supply to lowland dry basins, debunking the outdated notion that mountain groundwater storage and supply is negligible. Our study provides further evidence for the relevance of MBR. This has significant implications for replenishing groundwater resources, particularly in aquifer basins located in arid and semi-arid regions and adjacent to mountains, such as the Adelaide Plains basin, South Australia (Bresciani et al., 2018), Upper San Pedro Basin and Sabino Creek, Arizona, USA (Ajami et al., 2011; Wahi et al., 2008) and Central Valley California, emphasizing the complementary role of focused groundwater recharge through river channels and diffuse recharge via fractured deep bedrocks.

In the Sierra Nevada aquifers, cosmogenic isotope studies linking snowmelt and annual aquifer recharge indicate a strong link between snowmelt and aquifer recharge and discharge in the mountains (Urióstegui et al., 2017). Additional evidence is provided by the increased age of groundwater contributing to the spring stream flow over the Sierra Nevada, consistent with increased temperature and reduced precipitation at high elevations (Manning et al., 2012). Thus, the high Sierra Nevada snowpack is essential for recharging mountain aquifers, which, in turn, contributes to the long-term recharge of deep, confined CV aquifers. Sierra Nevada runoff and MFR's role in the freshwater supply in the CV is well-understood (Faunt, 2009; Meixner et al., 2016). However, the mountain block recharge process proposed here to replenish deep aquifers is not considered in the current hydrological models for the Valley, for example, by Faunt et al. (2009). Annual, interannual, and long-term changes in snowpack directly impact the MFR and MBR from the Sierra Nevada to the CV. Thus, the reliance on hydroclimate models that currently do not account for MBR limits the ability to accurately forecast the risk of climate extremes to California's groundwater supply and presents challenges for developing appropriate adaptation and resiliency strategies. The observation and analysis presented here have implications for the CV's recharge mechanism to deep aquifers. We call for new models that more comprehensively account for the Sierra Nevada's role in California's water cycle, which may also require a revision of current management and resiliency plans. Our analysis demonstrates that well level and deformation changes at seasonal time scales in the CV are also driven by a change in pressure, not only in storage. This conclusion is important for assumptions made in models that apply storage coefficients to groundwater level changes or deformation data to calculate groundwater storage change. Such models might only be applicable at long-term, but not at the seasonal time scales if snowmelt in the Sierra Nevada acts as a seasonal pressure regulator for the CV via MBR paths. Therefore, we also suggest the integration of pressure physics into methods quantifying seasonal storage changes in CV aquifers.

Data Availability

All data used for this study are publicly available from the following sources. GRACE JPL Mascon data were accessed from JPL PO.DAAC (Wiese et al., 2019). SNODAS data were downloaded from the National Snow & Ice Data Center (NOHRSC, 2004). GLDAS model outputs for Noah, CLSM, and VIC were retrieved from the Goddard Earth Sciences Data and Information Services Center (Beaudoing et al., 2016). We kindly thank Hannes Müller Schmied (hannes.mueller.schmied@em.uni-frankfurt.de) at the University of Frankfurt for providing WGHM version 2.2d outputs. GNSS time series were downloaded from the Nevada Geodetic Laboratory (Blewitt et al., 2018). The California Department of Water Resources provides reservoir data (CDWR, 2017) and groundwater level data. We retrieved all groundwater well sites within the study area as a bulk download from the California Natural Resources Agency via the California Open Data Portal for "Periodic Groundwater Level Measurements" (CDWR, 2019b) and for "Continuous Groundwater Level Measurements" (CDWR, 2019a). Further, we collected all groundwater level data available in the study region from the USGS archives (USGS, 2021) from the categories "Daily Data" and "Field Measurements". Open-source wavelet software packages were retrieved from by C. Torrence and G. Compo (Torrence & Compo, 1998 andon Erickson (Erickson, 2019). InSAR results, assembled groundwater records, and all data analysis results are presented in the supporting information or figures. They are made additionally available as data files through a repository with the Virginia Tech Data Repository (*to be defined*).

Author contribution

SW contributed with conceptualization, methodology, investigation, visualization, supervision and writing of the original draft as well as review and editing of the manuscript. MS contributed with conceptualization, methodology, investigation as well as review and editing of the manuscript. GC contributed with investigation. GC and RB contributed to reviewing and editing of the manuscript.

Competing interests

The authors declare that they have no conflict of interest.

Acknowledgments

We thank reviewers and editors for their constructive comments and suggestions. This research was partly funded by the National Aeronautics and Space Administration grants NNX17AD98G (SW, MS, GC), 80NSSC21K0419 (SW, MS, GC), and 80NSSC21K0061 (SW), as well as the Department of Energy grant DE-SC0019307 (MS).

References

Adusumilli, S., Borsa, A. A., Fish, M. A., McMillan, H. K., & Silverii, F. (2019). A decade of terrestrial water storage changes across the contiguous United States from GPS and GRACE. *Geophysical Research Letters*, 2019GL085370. https://doi.org/10.1029/2019GL085370

AghaKouchak, A., Chiang, F., Huning, L. S., Love, C. A., Mallakpour, I., Mazdiyasni, O., Moftakhari, H., Papalexiou, S. M., Ragno, E., & Sadegh, M. (2020). Climate Extremes and Compound Hazards in a Warming World. *Annual Review of Earth and Planetary Sciences*, *48*.

Ajami, H., Troch, P. A., Maddock, T., Meixner, T., & Eastoe, C. (2011). Quantifying mountain block recharge by means of catchment-scale storage-discharge relationships. *Water Resources Research*, *47*(4). https://doi.org/10.1029/2010WR009598

Alam, S., Gebremichael, M., Ban, Z., Scanlon, B. R., Senay, G., & Lettenmaier, D. P. (2021). Post-Drought Groundwater Storage Recovery in California's Central Valley. *Water Resources Research*, *57*(10). https://doi.org/10.1029/2021WR030352

Alley, W. M. (2002). Flow and Storage in Groundwater Systems. *Science*, *296*(5575), 1985–1990. https://doi.org/10.1126/science.1067123

Argus, D. F., Landerer, F. W., Wiese, D. N., Martens, H. R., Fu, Y., Famiglietti, J. S., Thomas, B. F., Farr, T. G., Moore, A. W., & Watkins, M. M. (2017). Sustained water loss in California's mountain ranges during severe drought from 2012 to 2015 inferred from GPS. *Journal of Geophysical Research: Solid Earth*, *122*(12), 10,510-559,585. https://doi.org/10.1002/2017JB014424

Argus, D. F., Martens, H. R., Borsa, A. A., Knappe, E., Wiese, D. N., Alam, S., Anderson, M., Khatiwada, A., Lau, N., Peidou, A., Swarr, M., White, A., Bos, M. S., Landerer, F. W., & Gardner, P. (2022). Subsurface water flux in California's Central Valley and its source watershed from space geodesy. *Geophysical Research Letters*. https://doi.org/10.1029/2022GL099583

Armengol, S., Ajami, H., Acero Triana, J. S., O. Sickman, J., & Ortega, L. (2024). Isogeochemical Characterization of Mountain System Recharge Processes in the Sierra Nevada, California. *Water Resources Research*, *60*(7). https://doi.org/10.1029/2023WR035719

Ayres, A., Hanak, E., Gray, B., Sencan, G., Bruno, E., Bou, A. E., & Collins, J. (2021). *Improving California' s Water Market*. https://www.ppic.org/publication/improving-californias-water-market/

Bales, R. C., Hopmans, J. W., O'Geen, A. T., Meadows, M., Hartsough, P. C., Kirchner, P., Hunsaker, C. T., & Beaudette, D. (2011). Soil Moisture Response to Snowmelt and Rainfall in a Sierra Nevada Mixed-Conifer Forest. *Vadose Zone Journal*, *10*(3), 786–799. https://doi.org/10.2136/vzj2011.0001

Beaudoing, H., Rodell, M., & NASA/GSFC/HSL. (2016). GLDAS Noah Land Surface Model L4 monthly 0.25 x 0.25 degree V2.1 [Dataset]. *Greenbelt, Maryland, USA, Goddard Earth Sciences Data and Information Services Center (GES DISC), Date Accessed: 2021-12-23*. https://doi.org/10.5067/SXAVCZFAQLNO

Berghuijs, W. R., Luijendijk, E., Moeck, C., van der Velde, Y., & Allen, S. T. (2022). Global Recharge Data Set Indicates Strengthened Groundwater Connection to Surface Fluxes. *Geophysical Research Letters*, *49*(23). https://doi.org/10.1029/2022GL099010

Blewitt, G., Hammond, W., & Kreemer, C. (2018). Harnessing the GPS Data Explosion for Interdisciplinary Science [Dataset]. *Eos, Date Accessed 2023-02-09*, *99*. https://doi.org/10.1029/2018EO104623

https://doi.org/10.5194/egusphere-2024-4023
Preprint. Discussion started: 19 March 2025

Borsa, A. A., Agnew, D. C., & Cayan, D. R. (2014). Ongoing drought-induced uplift in the western United States. *Science*, *345*(6204), 1587–1590. https://doi.org/10.1126/science.1260279

Bresciani, E., Cranswick, R. H., Banks, E. W., Batlle-Aguilar, J., Cook, P. G., & Batelaan, O. (2018). Using hydraulic head, chloride and electrical conductivity data to distinguish between mountain-front and mountain-block recharge to basin aquifers. *Hydrology and Earth System Sciences*, *22*(2), 1629–1648. https://doi.org/10.5194/hess-22-1629-2018

Brush, C. F., Dogrul, E. C., & Kadir, T. N. (2013). Development and Calibration of the California Central Valley Groundwater-Surface Water Simulation Model (C2VSim), Version 3.02-CG. In *California Department of Water Resources Technical Memorandum* (DWR Technical Memorandum). California Department of Water Resources. http://baydeltaoffice.water.ca.gov/modeling/hydrology/c2vsim/index_c2vsim.cfm

Burow, K. R., Dubrovsky, N. M., & Shelton, J. L. (2007). Temporal trends in concentrations of DBCP and nitrate in groundwater in the eastern San Joaquin Valley, California, USA. *Hydrogeology Journal*, *15*(5), 991–1007. https://doi.org/10.1007/s10040-006-0148-7

Carlson, G., Shirzaei, M., Ojha, C., & Werth, S. (2020). Subsidence-Derived Volumetric Strain Models for Mapping Extensional Fissures and Constraining Rock Mechanical Properties in the San Joaquin Valley, California. *Journal of Geophysical Research: Solid Earth*. https://doi.org/10.1029/2020JB019980

Carlson, G., Shirzaei, M., Werth, S., Zhai, G., & Ojha, C. (2020). Seasonal and Long-Term Groundwater Unloading in the Central Valley Modifies Crustal Stress. *Journal of Geophysical Research: Solid Earth*, *125*(1), 1–17. https://doi.org/10.1029/2019JB018490

Carlson, G., Werth, S., & Shirzaei, M. (2022). Joint Inversion of GNSS and GRACE for Terrestrial Water Storage Change in California. *Journal of Geophysical Research: Solid Earth*, *127*(3). https://doi.org/10.1029/2021JB023135

CDWR. (2017). *California Department of Water Resources, California Data Exchange Center, Active Monthly Reservoirs [Dataset]*. Data Accessed 2020-11-22. http://cdec.water.ca.gov/misc/monthly_res.html

CDWR. (2019a). *Continuous Groundwater Level Measurements [Dataset]*. Date Accessed 2019-12-18. https://data.ca.gov/dataset/continuous-groundwater-level-measurements

CDWR. (2019b). *Periodic Groundwater Level Measurements, California Department of Water Resources [Dataset]*. Date Accessed 2019-12-18. https://data.cnra.ca.gov/dataset/periodic-groundwater-level-measurements

Chanard, K., Métois, M., Rebischung, P., & Avouac, J. P. (2020). A warning against over-interpretation of seasonal signals measured by the Global Navigation Satellite System. *Nature Communications*, *11*(1), 1–4. https://doi.org/10.1038/s41467-020-15100-7

Costantini, M. (1998). A novel phase unwrapping method based on network programming. *IEEE Transactions on Geoscience and Remote Sensing*, *36*(3), 813–821. https://doi.org/10.1109/36.673674

Dillon, P. (2005). Future management of aquifer recharge. *Hydrogeology Journal*, *13*(1), 313–316. https://doi.org/10.1007/s10040-004-0413-6

Earman, S., Campbell, A. R., Phillips, F. M., & Newman, B. D. (2006). Isotopic exchange between snow and atmospheric water vapor: Estimation of the snowmelt component of groundwater recharge in the southwestern United States. *Journal of Geophysical Research Atmospheres*, *111*(9). https://doi.org/10.1029/2005JD006470

Erickson, J. (2019). *Continuous wavelet transform and inverse [Software]* (Retrieved August 30, 2019.). MATLAB Central File Exchange. https://www.mathworks.com/matlabcentral/fileexchange/20821-continuous-wavelet-transform-and-inverse

Escriva-Bou, A., Hui, R., Maples, S., Medellín-Azuara, J., Harter, T., & Lund, J. R. (2020). Planning for groundwater sustainability accounting for uncertainty and costs: An application to California's Central Valley. *Journal of Environmental Management*, *264*, 110426.

Escriva-Bou, A., Sencan, G., & Hanak, E. (2021). *Groundwater Recharge, Fact Sheet August 2021*. https://www.ppic.org/publication/groundwater-recharge/

Famiglietti, J. S., Lo, M., Ho, S. L., Bethune, J., Anderson, K. J., Syed, T. H., Swenson, S. C., de Linage, C. R., & Rodell, M. (2011). Satellites measure recent rates of groundwater depletion in California's Central Valley. *Geophysical Research Letters*, *38*(3). https://doi.org/10.1029/2010GL046442

Farr, T. G., Rosen, P. A., Caro, E., Crippen, R., Duren, R., Hensley, S., Kobrick, M., Paller, M., Rodriguez, E., Roth, L., Seal, D., Shaffer, S., Shimada, J., Umland, J., Werner, M., Oskin, M., Burbank, D., & Alsdorf, D. (2007). The Shuttle Radar Topography Mission. *Reviews of Geophysics*, *45*(2), RG2004. https://doi.org/10.1029/2005RG000183

Faunt, C. C. (2009). *Groundwater Availability of the Central Valley Aquifer, California* (C. C. Faunt, Ed.). U.S. Geological Survey Professional Paper 1766. https://pubs.usgs.gov/pp/1766/

Faunt, C. C., Sneed, M., Traum, J., & Brandt, J. T. (2016). Water availability and land subsidence in the Central Valley, California, USA. *Hydrogeology Journal*, *24*(3), 675–684. https://doi.org/10.1007/s10040-015-1339-x

Feth, J. H. (1964). Hidden Recharge. *Groundwater*, *2*(4), 14–17. https://doi.org/10.1111/j.1745-6584.1964.tb01780.x

Fetter, C. W., & Kreamer, D. (2022). *Applied Hydrogeology* (5th ed.). Waveland Press.

Fox-Kemper, B., Hewitt, H. T., Xiao, C., Aðalgeirsdóttir, G., Drijfhout, S. S., Edwards, T. L., Golledge, N. R., Hemer, M., Kopp, R. E., Krinner, G., Mix, A., Notz, D., Nowicki, S., Nurhati, I. S., Ruiz, L., Sallée, J.-B., Slangen, A. B. A., & Yu, Y. (2021). Ocean, Cryosphere and Sea Level Change. In *Climate Change 2021: The Physical Science Basis. Contribution of Working Group I to the Sixth Assessment Report of the Intergovernmental Panel on Climate Change [MassonDelmotte, et al. (eds.)]*. Cambridge University Press. https://doi.org/10.1017/9781009157896

Franceschetti, G., & Lanari, R. (1999). *Synthetic aperture radar processing*. CRC Press.

Galloway, D. L., Jones, D. R., & Ingebritsen, S. E. (1999). *Land subsidence in the United States*. U.S. Geological Survey Circular 1182. https://doi.org/10.3133/cir1182

Gao, S. S., Silver, P. G., Linde, A. T., & Sacks, I. S. (2000). Annual modulation of triggered seismicity following the 1992 Landers earthquake in California. *Nature*, *406*(6795), 500–504. https://doi.org/10.1038/35020045

Gardner, P., & Heilweil, V. (2009). *Evaluation of the effects of precipitation on ground-water levels from wells in selected alluvial aquifers in Utah and Arizona, 1936-2005*. https://doi.org/10.3133/sir20085242

Ghasemizade, M., Asante, K. O., Petersen, C., Kocis, T., Dahlke, H. E., & Harter, T. (2019). An Integrated Approach Toward Sustainability via Groundwater Banking in the Southern Central Valley, California. *Water Resources Research*, *55*(4), 2742–2759. https://doi.org/10.1029/2018WR024069

Gilbert, J. M., & Maxwell, R. M. (2017). Examining regional groundwater-surface water dynamics using an integrated hydrologic model of the San Joaquin River basin. *Hydrology and Earth System Sciences*, *21*(2), 923–947. https://doi.org/10.5194/hess-21-923-2017

Goswami, J. C., & Chan, A. K. (1999). *Fundamentals of Wavelets: Theory, Algorithms, and Applications*. Wiley-Interscience.

Hanak, E., Lund, J., Arnold, B., Escriva-Bou, A., Gray, B., Green, S., Harter, T., Howitt, R., MacEwan, D., & Medellín-Azuara, J. (2017). *Water Stress and a Changing San Joaquin Valley*. Public Policy Institute of California. https://www.ppic.org/publication/water-stress-and-a-changing-san-joaquin-valley/

Hanson, R. T., Flint, L. E., Flint, A. L., Dettinger, M. D., Faunt, C. C., Cayan, D., & Schmid, W. (2012). A method for physically based model analysis of conjunctive use in response to potential climate changes. *Water Resources Research*, *48*(2). https://doi.org/10.1029/2011WR010774

Harpold, A., Dettinger, M., & Rajagopal, S. (2017). Defining Snow Drought and Why It Matters. *Eos*. https://doi.org/10.1029/2017EO068775

Hatchett, B. J., & McEvoy, D. J. (2018). Exploring the origins of snow drought in the northern sierra nevada, california. *Earth Interactions*, *22*(2), 1–13. https://doi.org/10.1175/EI-D-17-0027.1

Huth, A. K., Leydecker, A., Sickman, J. O., & Bales, R. C. (2004). A two-component hydrograph separation for three high-elevation catchments in the Sierra Nevada, California. *Hydrological Processes*, *18*(9), 1721–1733. https://doi.org/10.1002/hyp.1414

Jakeman, A. J., Barreteau, O., Hunt, R. J., Rinaudo, J.-D., Ross, A., Arshad, M., & Hamilton, S. (2016). Integrated Groundwater Management: An Overview of Concepts and Challenges. In *Integrated Groundwater Management* (pp. 3–20). Springer International Publishing. https://doi.org/10.1007/978-3-319-23576-9_1

Jódar, J., Cabrera, J. A., Martos-Rosillo, S., Ruiz-Constán, A., González-Ramón, A., Lambán, L. J., Herrera, C., & Custodio, E. (2017). Groundwater discharge in high-mountain watersheds: A valuable resource for downstream semi-arid zones. The case of the Bérchules River in Sierra Nevada (Southern Spain). *Science of The Total Environment*, *593–594*, 760–772. https://doi.org/10.1016/j.scitotenv.2017.03.190

Johnson, C. W., Fu, Y., & Bürgmann, R. (2017). Seasonal water storage, stress modulation, and California seismicity. *Science*, *356*(6343), 1161–1164. https://doi.org/10.1126/science.aak9547

Konikow, L. F. (2015). Long-Term Groundwater Depletion in the United States. *Groundwater*, *53*(1), 2–9. https://doi.org/10.1111/gwat.12306

Kourakos, G., Brunetti, G., Bigelow, D. P., Wallander, S., & Dahlke, H. E. (2023). Optimizing Managed Aquifer Recharge Locations in California's Central Valley Using an Evolutionary Multi-Objective Genetic Algorithm Coupled With a Hydrological Simulation Model. *Water Resources Research*, *59*(5). https://doi.org/10.1029/2022WR034129

Kourakos, G., Dahlke, H. E., & Harter, T. (2019). Increasing Groundwater Availability and Seasonal Base Flow Through Agricultural Managed Aquifer Recharge in an Irrigated Basin. *Water Resources Research*, *55*(9), 7464–7492. https://doi.org/10.1029/2018WR024019

Kuss, A. J. M., & Gurdak, J. J. (2014). Groundwater level response in U.S. principal aquifers to ENSO, NAO, PDO, and AMO. *Journal of Hydrology*, *519*(PB), 1939–1952. https://doi.org/10.1016/j.jhydrol.2014.09.069

Lee, J. C., & Shirzaei, M. (2023). Novel algorithms for pair and pixel selection and atmospheric error correction in multitemporal InSAR. *Remote Sensing of Environment*, *286*. https://doi.org/10.1016/j.rse.2022.113447

Li, R., Ou, G., Pun, M., & Larson, L. (2018). Evaluation of Groundwater Resources in Response to Agricultural Management Scenarios in the Central Valley, California. *Journal of Water Resources Planning and Management*, *144*(12), 04018078. https://doi.org/10.1061/(asce)wr.1943-5452.0001014

Liu, F., Conklin, M. H., & Shaw, G. D. (2017). Insights into hydrologic and hydrochemical processes based on concentration-discharge and end-member mixing analyses in the mid-Merced River Basin, Sierra Nevada, California. *Water Resources Research*, *53*(1), 832–850. https://doi.org/10.1002/2016WR019437

Manning, A. H., Clark, J. F., Diaz, S. H., Rademacher, L. K., Earman, S., & Niel Plummer, L. (2012). Evolution of groundwater age in a mountain watershed over a period of thirteen years. *Journal of Hydrology*, *460–461*, 13–28. https://doi.org/10.1016/j.jhydrol.2012.06.030

Markovich, K. H., Manning, A. H., Condon, L. E., & McIntosh, J. C. (2019). Mountain-Block Recharge: A Review of Current Understanding. *Water Resources Research*, *55*(11), 8278–8304. https://doi.org/10.1029/2019WR025676

Marwaha, N., Kourakos, G., Levintal, E., & Dahlke, H. E. (2021). Identifying Agricultural Managed Aquifer Recharge Locations to Benefit Drinking Water Supply in Rural Communities. *Water Resources Research*, *57*(3). https://doi.org/10.1029/2020WR028811

Massoud, E. C., Purdy, A. J., Miro, M. E., & Famiglietti, J. S. (2018). Projecting groundwater storage changes in California's Central Valley. *Scientific Reports*, *8*(1), 12917. https://doi.org/10.1038/s41598-018-31210-1

McCabe, G. J., Palecki, M. A., & Betancourt, J. L. (2004). Pacific and Atlantic Ocean influences on multidecadal drought frequency in the United States. *Proceedings of the National Academy of Sciences*, *101*(12), 4136–4141. https://doi.org/10.1073/pnas.0306738101

McMahon, P. B., Plummer, L. N., Böhlke, J. K., Shapiro, S. D., & Hinkle, S. R. (2011). A comparison of recharge rates in aquifers of the United States based on groundwater-age data. *Hydrogeology Journal*, *19*(4), 779–800. https://doi.org/10.1007/s10040-011-0722-5

Meixner, T., Manning, A. H., Stonestrom, D. A., Allen, D. M., Ajami, H., Blasch, K. W., Brookfield, A. E., Castro, C. L., Clark, J. F., & Gochis, D. J. (2016). Implications of projected climate change for groundwater recharge in the western United States. *Journal of Hydrology*, *534*, 124–138.

Meixner, T., Manning, A. H., Stonestrom, D. A., Allen, D. M., Ajami, H., Blasch, K. W., Brookfield, A. E., Castro, C. L., Clark, J. F., Gochis, D. J., Flint, A. L., Neff, K. L., Niraula, R., Rodell, M., Scanlon, B. R., Singha, K., & Walvoord, M. A. (2015). Implications of Projected Climate Change for Groundwater Recharge in the Western United. *Journal of Hydrology*, *534*, 124–138. https://doi.org/10.1016/j.jhydrol.2015.12.027

Meyer, P. L. (1970). *Introductory Probability and Statistical Applicaitons* (2nd ed.). Oxford & IBH Publishing Co.

Montgomery-Brown, E. K., Shelly, D. R., & Hsieh, P. A. (2019). Snowmelt-Triggered Earthquake Swarms at the Margin of Long Valley Caldera, California. *Geophysical Research Letters*, *46*(7), 3698–3705. https://doi.org/10.1029/2019GL082254

Mote, P. W., Li, S., Lettenmaier, D. P., Xiao, M., & Engel, R. (2018). Dramatic declines in snowpack in the western US. *Npj Climate and Atmospheric Science*, *1*(1). https://doi.org/10.1038/s41612-018-0012-1

Neely, W. R., Borsa, A. A., Burney, J. A., Levy, M. C., Silverii, F., & Sneed, M. (2021). Characterization of Groundwater Recharge and Flow in California's San Joaquin Valley From InSAR-Observed Surface Deformation. *Water Resources Research*, *57*(4), 1–20. https://doi.org/10.1029/2020wr028451

Neely, W. R., Knight, R., Kang, S., & Goebel, M. (2024). Exploring the InSAR signature associated with river-sourced recharge in California's San Joaquin Valley. *Environmental Research Letters*. https://doi.org/10.1088/1748-9326/ad5855

NOHRSC. (2004). *National Operational Hydrologic Remote Sensing Center, Snow Data Assimilation System (SNODAS) data products at NSIDC. Version 1. [Dataset]*. National Snow and Ice Data Center, Boulder, CO, USA, Date Accessed 2020-11-21. https://doi.org/10.7265/N5TB14TC

Ojha, C., Shirzaei, M., Werth, S., Argus, D. F., & Farr, T. G. (2018). Sustained Groundwater Loss in California's Central Valley Exacerbated by Intense Drought Periods. *Water Resources Research*, *54*(7), 4449–4460. https://doi.org/10.1029/2017WR022250

Ojha, C., Werth, S., & Shirzaei, M. (2019). Groundwater Loss and Aquifer System Compaction in San Joaquin Valley During 2012–2015 Drought. *Journal of Geophysical Research: Solid Earth*, *124*(3), 3127–3143. https://doi.org/10.1029/2018JB016083

Pepin, N., Bradley, R. S., Diaz, H. F., Baraer, M., Caceres, E. B., Forsythe, N., Fowler, H., Greenwood, G., Hashmi, M. Z., Liu, X. D., Miller, J. R., Ning, L., Ohmura, A., Palazzi, E., Rangwala, I., Schöner, W., Severskiy, I., Shahgedanova, M., Wang, M. B., … Yang, D. Q. (2015). Elevation-dependent warming in mountain regions of the world. *Nature Climate Change*, *5*(5), 424–430. https://doi.org/10.1038/nclimate2563

Perrone, D., & Jasechko, S. (2019). Deeper well drilling an unsustainable stopgap to groundwater depletion. *Nature Sustainability*, *2*(8), 773–782. https://doi.org/10.1038/s41893-019-0325-z

Peterson, D., Smith, R., Stewart, I., Knowles, N., Soulard, C., Hager, S., & Norton, G. A. (2003). *Snowmelt Discharge Characteristics, Sierra Nevada, California.* (Series Name SIR - 2005-5056). U.S. Geological Survey.

https://doi.org/10.5194/egusphere-2024-4023
Preprint. Discussion started: 19 March 2025

Quiring, S. M., & Goodrich, G. B. (2008). Nature and causes of the 2002 to 2004 drought in the southwestern United States compared with the historic 1953 to 1957 drought. *Climate Research*, *36*(1), 41–52. https://doi.org/10.3354/cr00735

Rodell, M., Houser, P. R., Jambor, U., Gottschalck, J., Mitchell, K., Meng, C.-J., Arsenault, K., Cosgrove, B., Radakovich, J., Bosilovich, M., Entin*, J. K., Walker, J. P., Lohmann, D., & Toll, D. (2004). The Global Land Data Assimilation System. *Bulletin of the American Meteorological Society*, *85*(3), 381–394. https://doi.org/10.1175/BAMS-85-3-381

Saar, M. O., & Manga, M. (2003). Seismicity induced by seasonal groundwater recharge at Mt. Hood, Oregon. *Earth and Planetary Science Letters*, *214*(3–4), 605–618. https://doi.org/10.1016/S0012-821X(03)00418-7

Scanlon, B. R., Longuevergne, L., & Long, D. (2012). Ground referencing GRACE satellite estimates of groundwater storage changes in the California Central Valley, USA. *Water Resources Research*, *48*(4), W04520. https://doi.org/10.1029/2011WR011312

Schmidt, R., Flechtner, F., Meyer, U., Neumayer, K.-H., Dahle, C., König, R., & Kusche, J. (2008). Hydrological Signals Observed by the GRACE Satellites. *Surveys in Geophysics*, *29*(4–5), 319–334. https://doi.org/10.1007/s10712-008-9033-3

Schreiner-McGraw, A. P., & Ajami, H. (2022). Combined impacts of uncertainty in precipitation and air temperature on simulated mountain system recharge from an integrated hydrologic model. *Hydrology and Earth System Sciences*, *26*(4), 1145–1164. https://doi.org/10.5194/hess-26-1145-2022

Shirzaei, M. (2013). A Wavelet-Based Multitemporal DInSAR Algorithm for Monitoring Ground Surface Motion. *Ieee Geoscience and Remote Sensing Letters*, *10*(3), 456–460. https://doi.org/Doi 10.1109/Lgrs.2012.2208935

Shirzaei, M., Bürgmann, R., & Fielding, E. J. (2017). Applicability of Sentinel-1 Terrain Observation by Progressive Scans multitemporal interferometry for monitoring slow ground motions in the San Francisco Bay Area. *Geophysical Research Letters*, *44*(6), 2733–2742. https://doi.org/10.1002/2017GL072663.

Shirzaei, M., Bürgmann, R., Foster, J., Walter, T. R., & Brooks, B. A. (2013). Aseismic deformation across the Hilina fault system, Hawaii, revealed by wavelet analysis of InSAR and GPS time series. *Earth and Planetary Science Letters*, *376*, 12–19. https://doi.org/10.1016/j.epsl.2013.06.011

Shirzaei, M., Ojha, C., Werth, S., Carlson, G., & Vivoni, E. R. (2019). Comment on "Short-lived pause in Central California subsidence after heavy winter precipitation of 2017" by K. D. Murray and R. B. Lohman. *Science Advances*, *5*(eaav8038). https://doi.org/10.1126/sciadv.aav8038

Siebert, S., Burke, J., Faures, J. M., Frenken, K., Hoogeveen, J., Döll, P., & Portmann, F. T. (2010). Groundwater use for irrigation - A global inventory. *Hydrology and Earth System Sciences*, *14*(10), 1863–1880. https://doi.org/10.5194/hess-14-1863-2010

Siirila-Woodburn, E. R., Dennedy-Frank, P. J., Rhoades, A., Vahmani, P., Maina, F., Hatchett, B., Zhou, Y., & Jones, A. (2023). The Role of Atmospheric Rivers on Groundwater: Lessons Learned From an Extreme Wet Year. *Water Resources Research*, *59*(6). https://doi.org/10.1029/2022WR033061

Siirila-Woodburn, E. R., Rhoades, A. M., Hatchett, B. J., Huning, L. S., Szinai, J., Tague, C., Nico, P. S., Feldman, D. R., Jones, A. D., Collins, W. D., & Kaatz, L. (2021). A low-to-no snow future and its impacts on water resources in the western

https://doi.org/10.5194/egusphere-2024-4023
Preprint. Discussion started: 19 March 2025

United States. In *Nature Reviews Earth and Environment* (Vol. 2, Issue 11, pp. 800–819). Springer Nature. https://doi.org/10.1038/s43017-021-00219-y

Smerdon, B. D. (2017). A synopsis of climate change effects on groundwater recharge. In *Journal of Hydrology* (Vol. 555, pp. 125–128). Elsevier B.V. https://doi.org/10.1016/j.jhydrol.2017.09.047

Smith, R. G., Knight, R., Chen, J., Reeves, J. A., Zebker, H. A., Farr, T., & Liu, Z. (2017). Estimating the permanent loss of groundwater storage in the southern San Joaquin Valley, California. *Water Resources Research*, *53*(3), 2133–2148. https://doi.org/10.1002/2016WR019861

Somers, L. D., & McKenzie, J. M. (2020). A review of groundwater in high mountain environments. *Wiley Interdisciplinary Reviews: Water*, *7*(6), 1–27. https://doi.org/10.1002/wat2.1475

Stevenson, S., Coats, S., Touma, D., Cole, J., Lehner, F., Fasullo, J., & Otto-Bliesner, B. (2022). Twenty-first century hydroclimate: A continually changing baseline, with more frequent extremes. *Proceedings of the National Academy of Sciences*, *119*(12). https://doi.org/10.1073/pnas.2108124119

Tague, C., & Grant, G. E. (2009). Groundwater dynamics mediate low-flow response to global warming in snow-dominated alpine regions. *Water Resources Research*, *45*(7). https://doi.org/10.1029/2008WR007179

Tague, C., Grant, G., Farrell, M., Choate, J., & Jefferson, A. (2008). Deep groundwater mediates streamflow response to climate warming in the Oregon Cascades. *Climatic Change*, *86*(1–2), 189–210. https://doi.org/10.1007/s10584-007-9294-8

Talwani, P., & Acree, S. (1985). Pore pressure diffusion and the mechanism of reservoir-induced seismicity. In *Earthquake prediction* (pp. 947–965). Springer.

Tang, Q., & Oki, T. (Eds.). (2016). *Terrestrial Water Cycle and Climate Change*. John Wiley & Sons, Inc. https://doi.org/10.1002/9781118971772

Tapley, B. D., Bettadpur, S., Ries, J. C., Thompson, P. F., & Watkins, M. M. (2004). GRACE measurements of mass variability in the Earth system. *Science*, *305*(5683), 503–505. https://doi.org/10.1126/science.1099192

Taylor, R. G. (2012). Ground water and climate change. *Nature Climate Change*, *3*, 322–329. https://doi.org/10.1038/NCLIMATE1744

Torrence, C., & Compo, G. P. (1998). A practical guide to wavelet analysis [Software]. In *Bulletin of the American Meteorological Society* (Retrieved December 5, 2018.; Vol. 79, Issue 1, pp. 61–78). https://doi.org/10.1175/1520-0477(1998)079<0061:APGTWA>2.0.CO;2

Urióstegui, S. H., Bibby, R. K., Esser, B. K., & Clark, J. F. (2017). Quantifying annual groundwater recharge and storage in the central Sierra Nevada using naturally occurring 35S. *Hydrological Processes*, *31*(6), 1382–1397. https://doi.org/10.1002/hyp.11112

USGS. (2021). *USGS Groundwater Data for the Nation [Dataset]*. Date Accessed: 2021-05-15. https://waterdata.usgs.gov/nwis/gw

Vasco, D. W., Kim, K., Farr, T. G., Reager, J. T., Bekaert, D., Singh, S., & Beaudoing, H. K. (2022). Using Sentinel-1 and GRACE satellite data to monitor the long- and short-term hydrological variations within the Tulare Basin , California. *Scientific Reports*, 1–14. https://doi.org/10.1038/s41598-022-07650-1

Visser, A., Moran, J. E., Singleton, M. J., & Esser, B. K. (2018). Importance of river water recharge to the San Joaquin Valley groundwater system. *Hydrological Processes*, *32*(9), 1202–1213. https://doi.org/10.1002/hyp.11468

Viswanathan, H. S., Ajo-Franklin, J., Birkholzer, J. T., Carey, J. W., Guglielmi, Y., Hyman, J. D., Karra, S., Pyrak-Nolte, L. J., Rajaram, H., Srinivasan, G., & Tartakovsky, D. M. (2022). From Fluid Flow to Coupled Processes in Fractured Rock: Recent Advances and New Frontiers. In *Reviews of Geophysics* (Vol. 60, Issue 1). John Wiley and Sons Inc. https://doi.org/10.1029/2021RG000744

Wahi, A. K., Hogan, J. F., Ekwurzel, B., Baillie, M. N., & Eastoe, C. J. (2008). Geochemical Quantification of Semiarid Mountain Recharge. *Ground Water*, *46*(3), 414–425. https://doi.org/10.1111/j.1745-6584.2007.00413.x

Wang, H. F. (2000). *Theory of Linear Poroelasticity with Applications to Geomechanics and Hydrogeology*. Princeton Univ. Press.

Welch, L. A., & Allen, D. M. (2014). Hydraulic conductivity characteristics in mountains and implications for conceptualizing bedrock groundwater flow. *Hydrogeology Journal*, *22*(5), 1003–1026. https://doi.org/10.1007/s10040-014-1121-5

Werner, C., U. Wegmüller, T. Strozzi, & A. Wiesmann. (2000). Gamma SAR and interferometric processing software. *Proceedings of the Ers-Envisat Symposium, Gothenburg, Sweden.*

White, A. M., Gardner, W. P., Borsa, A. A., Argus, D. F., & Martens, H. R. (2022). A review of GNSS/GPS in hydrogeodesy: Hydrologic loading applications and their implications for water resource research. *Water Resources Research*. https://doi.org/10.1029/2022WR032078

Wiese, D. N., Yuan, D.-N., Boening, C., Landerer, F. W., & Watkins, M. M. (2019). *JPL GRACE and GRACE-FO Mascon Ocean, Ice, and Hydrology Equivalent Water Height CRI Filtered. Ver. RL06Mv02 [Dataset]*. PO.DAAC, CA, USA, Date Accessed 2021-12-23. https://doi.org/10.5067/TEMSC-3JC62

Yang, K., Rittger, K., Musselman, K. N., Bair, E. H., Dozier, J., Margulis, S. A., Painter, T. H., & Molotch, N. P. (2023). Intercomparison of snow water equivalent products in the Sierra Nevada California using airborne snow observatory data and ground observations. *Frontiers in Earth Science*, *11*. https://doi.org/10.3389/feart.2023.1106621

Zektser, I. S., & Everett, L. G. (2004). *Groundwater Resources ofthe World and Their Use* (IHP-VI Series on Groundwater No. 6). United Nations Educational, Scientific and Cultural Organization (UNESCO). https://b-ok.org/book/610713/027e58

Zhai, G., Shirzaei, M., Manga, M., & Chen, X. (2019). Pore-pressure diffusion, enhanced by poroelastic stresses, controls induced seismicity in Oklahoma. *Proceedings of the National Academy of Sciences*, 201819225. https://doi.org/10.1073/pnas.1819225116

Zheng, Y., Ross, A., Villholth, K. G., & Dillon, P. (Eds.). (2021). *Managing Aquifer Recharge: A Showcase for Resilience and Sustainability*. UNESCO. https://unesdoc.unesco.org/ark:/48223/pf0000379962